Gondwana Research 35 (2016) 97–114

Contents lists available at ScienceDirect

Gondwana Research

journal homepage: www.elsevier.com/locate/gr

Tectonic drivers and the influence of the Kerguelen plume on seafloor spreading during formation of the early Indian Ocean

S.J. Watson [a,*], J.M. Whittaker [a], J.A. Halpin [a,b], S.E. Williams [c], L.A. Milan [d], N.R. Daczko [e], D.A. Wyman [c]

[a] Institute for Marine and Antarctic Studies, University of Tasmania, Private Bag 129, Hobart, Tasmania 7001, Australia
[b] ARC Centre of Excellence in Ore Deposits (CODES), School of Physical Sciences, University of Tasmania, Private Bag 79, Tasmania 7001, Australia
[c] Earthbyte Group, School of Geosciences, University of Sydney, Sydney, New South Wales, 2006, Australia
[d] Division of Earth Sciences, School of Environmental and Rural Science, University of New England, Armidale, New South Wales 2351, Australia
[e] Department of Earth and Planetary Sciences, Macquarie University 2109, New South Wales, Australia

ARTICLE INFO

Article history:
Received 7 August 2015
Received in revised form 6 March 2016
Accepted 17 March 2016
Available online 2 May 2016

Handling Editor: A.R.A. Aitken

Keywords:
Extinct ridge
Plate motion
Kerguelen
Trace geochemistry
East Gondwana
Dirck Hartog Ridge

ABSTRACT

The Perth Abyssal Plain (PAP), located offshore southwest Australia, formed at the centre of Mesozoic East Gondwana breakup and Kerguelen plume activity. Despite its importance as a direct and relatively undisturbed recorder of this early spreading history, sparse geophysical data sets and lack of geological sampling hamper our understanding of the evolution of the PAP. This study combines new bathymetric profiles across the PAP with petrographic and geochemical data from the first samples ever to be dredged from the flanks of the Dirck Hartog Ridge (DHR), a prominent linear bathymetric feature in the central PAP, to better constrain the formation of the early Indian Ocean floor and the influence of the Kerguelen plume. Seafloor spreading in the PAP initiated at ~136 Ma with spreading observed to occur at (half) rates of ~35 mm/yr. Changes in spreading rate are difficult to discern after the onset of the Cretaceous Quiet Zone at ~120 Ma, but an increase in seafloor roughness towards the centre of the PAP likely resulted from a half-spreading rate decrease from 35 mm/yr (based on magnetic reversals) to ~24 mm/yr at ~114 Ma. Exhumed gabbro dredged from the southernmost dredge site of the DHR supports a further slowdown of spreading immediately prior to full cessation at ~102 Ma. The DHR exhibits a high relief ridge axis and distinctive asymmetry that is unusual compared to most active or extinct spreading centres. The composition of mafic volcanic samples varies along the DHR, from sub-alkaline dolerites with incompatible element concentrations most similar to depleted-to-normal mid-ocean ridge basalts in the south, to alkali basalts similar to ocean island basalts in the north. Therefore, magma sources and degrees of partial melting varied in space and time. It is likely that the alkali basalts are a manifestation of later excess volcanism, subsequent to or during the cessation of spreading. In this case, enriched signatures may be attributed tectonic drivers and melting of a heterogeneous mantle, or to an episodic influence of the Kerguelen plume over distances greater than 1000 km. We also investigate possible scenarios to explain how lower crustal rocks were emplaced at the crest of the southern DHR. Our results demonstrate the significance of regional tectonic plate motions on the formation and deformation of young ocean crust, and provide insight into the unique DHR morphology.

1. Introduction

The Perth Abyssal Plain (PAP), offshore Western Australia (Fig. 1), was at the nexus of Mesozoic East Gondwana breakup between Australia, Antarctic, and India. The PAP and the Enderby Basin (Fig. 1) formed a continuous spreading system following continental rifting and breakup between India and Australia (from ~136 Ma) and continued during the formation of the nearby Southern (110–118 Ma) and Central (105–95 Ma) Kerguelen Plateaux (Gibbons et al., 2012). Despite its importance as a direct and relatively undisturbed recorder of this early spreading history, sparse geophysical data sets and lack of geological sampling hamper our understanding of the evolution of the PAP. Obtaining good geophysical and geological data in the PAP is critical to understanding the early evolution of the eastern Indian Ocean as primary seafloor morphology is masked by widespread Kerguelen-related volcanism in the Enderby Basin (Fig. 1; Gaina et al., 2007), the conjugate ocean floor (offshore Greater India) is obscured through the process of subduction beneath Southeast Asia and thick sediment cover in the Bay of Bengal (Divins, 2003; Krishna et al., 2009; Williams et al., 2013). Further difficulties are caused by much of the PAP ocean floor having formed within the Cretaceous Quiet Zone (CQZ; Williams et al., 2013), during which there is an absence of magnetic anomaly reversals with which to constrain seafloor spreading.

A scientific voyage on the *R/V Southern Surveyor* in 2011 (SS2011_V06) acquired magnetic and bathymetric data across the

* Corresponding author.
E-mail address: sally.watson@utas.edu.au (S.J. Watson).

http://dx.doi.org/10.1016/j.gr.2016.03.009
1342-937X/

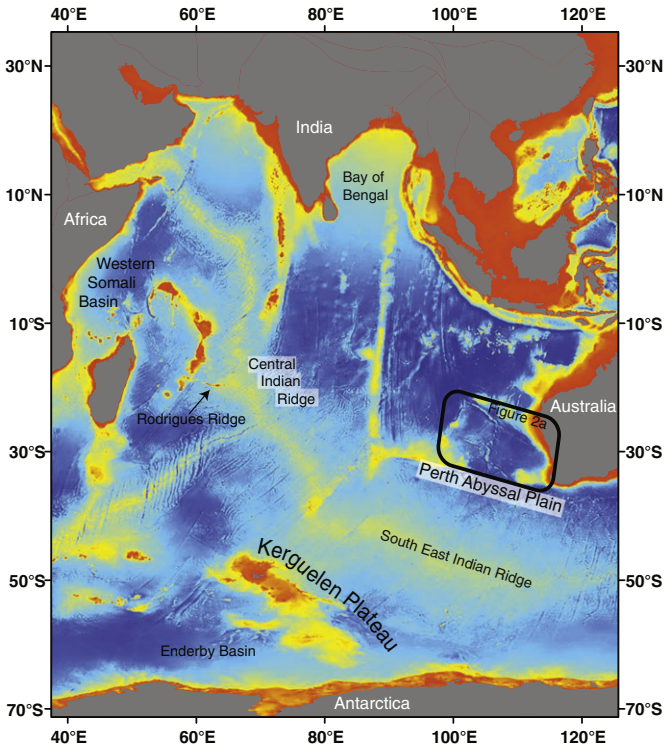

Fig. 1. Present day regional bathymetric map of the Indian Ocean (*Etopo 2v2*; NOAA, 2006), continents are in gray. The Perth Abyssal Plain study area is outlined in the black rectangle (also representing the location of Fig. 2a), and features referred to in the text are labelled.

PAP. During this voyage, geological material was dredged from the previously unsampled Batavia and Gulden Draak knolls, now newly identified as microcontinents (Gardner et al., 2015), and the Dirck Hartog Ridge (DHR), an enigmatic linear bathymetric feature, oriented approximately north–south, located in the centre of the PAP (Fig. 2a; Williams, 2011). Williams et al. (2013) interpreted the new magnetic anomaly data to constrain the Mesozoic seafloor spreading in the PAP and suggested that multiple ridge jumps were likely caused by the proximal Kerguelen plume (Fig. 2a).

In this study, we use the new bathymetric data and geochemical results to reveal a complex tectonic history for the PAP and formation of the DHR. We present the first results from mafic igneous samples dredged from the flanks of the DHR (Sites 5, 6, and 7; Fig. 2b). We investigate the tectonic evolution of the DHR, detailing the timing and complex geological processes involved during the cessation of spreading, and explain the unusual morphology of the DHR. The bathymetric data and geochemical results presented here enable us to revise the evolution of the latter stages of spreading and cessation of the PAP. We evaluate the influence of contemporaneous Kerguelen plume-related magmatic upwelling and tectonic plate reorganisation on the morphology and volcanism on the DHR. Our results provide new insights into the geodynamic processes associated with seafloor spreading in the PAP and contribute to a greater understanding of the complex history of Mesozoic seafloor spreading between India and Australia during East Gondwanan dispersion.

2. Tectonic setting

2.1. Breakup of East Gondwana and the formation of the Perth Abyssal Plain

Breakup of East Gondwana initiated as Argoland rifted from the northwest Australian margin forming the Argo Abyssal Plain from ~155 Ma (Gibbons et al., 2012). In the Early Cretaceous, rifting propagated southward separating India from Australia-Antarctica, progressively forming the western margin of Australia, and the Cuvier and Gascoyne Abyssal Plains (Fig. 2a; Müller et al., 2000; Gibbons et al., 2012, 2013). Spreading initiated in the PAP by at least M10 (~130 Ma) with extension of spreading rates to the continent–ocean boundary (Gibbons et al., 2012; Whittaker et al., 2013) and an interpreted Valanginian breakup unconformity (Crostella and Backhouse, 2000; Jones et al., 2012) supporting breakup at ~136–7 Ma. At this time, the PAP and the Enderby Basin (now located on the Antarctic plate; Fig. 1) formed one diverging plate boundary between India and Australia-Antarctica (Gaina et al., 2007). A number of microcontinental fragments (Wallaby and Zenith plateaux, and the Gulden Draak and Batavia knolls) on the West Australian margin, as well as the Elan Bank (the western salient of the Kerguelen Plateau) in the Enderby Basin, were isolated by a series of westward ridge jumps between 130 Ma and 100 Ma (Fig. 2a; Mihut and Müller, 1998; Müller et al., 2000; Gibbons et al., 2013).

In the PAP, magnetic anomalies interpreted prior to the onset of the CQZ (M0; ~121 Ma) are used to determine a minimum constraint for the onset of seafloor spreading (M10; 130 Ma; Williams et al., 2013). Based on these interpreted magnetic anomalies, early spreading progressed at an intermediate rate (~35 mm/yr half spreading rate; Gibbons et al., 2012; Williams et al., 2013). Magnetic anomalies decrease in age towards the centre of the PAP and conjugate anomalies in the East and West PAP suggest the presence of at least two extinct spreading centres in the PAP (Fig. 2a) (Williams et al., 2013).

The Mesozoic magnetic anomalies in the East PAP show the repetition of M0 (~121 Ma; Fig. 2a), indicating a ridge jump occurred at ~M0 after formation of ~600 km of ocean crust, relocating the ridge axis ~200 km to the west (Williams et al., 2013). Another westward ridge jump from the PAP to the Wharton Basin at 101–104 Ma (Whittaker et al., in review) marked the cessation of spreading in the PAP and effectively isolated microcontinental fragments Batavia and Gulden Draak Knolls (Müller et al., 1998; Kobler, 2012; Whittaker et al., 2013; Gardner et al., 2015).

Coeval with and proximal to PAP formation (130–101/104 Ma), the Kerguelen plume extruded over 1.3×10^7 km^3 of volcanic rock (Coffin et al., 2002). Kerguelen plume volcanism prior to the formation of the South Kerguelen Plateau (110–119 Ma) was widespread. For example, the onshore Tibetan Comei Large Igneous Province and the Western Australian Bunbury Basalts are both attributed to the early Kerguelen plume (Frey et al., 1996; Zhu et al., 2009). The profuse influence of the Kerguelen plume suggests a long-term incubation of the plume beneath East Gondwana, commencing with relatively low-supply interspersed continental volcanism and increasing dramatically during the formation of the South Kerguelen Plateau (Coffin et al., 2002). At the peak of its production (119–100 Ma), the Kerguelen plume extruded vast voluminous volcanic sequences forming the Southern and Central Kerguelen Plateaux (including the Elan Bank; Frey et al., 2000; Coffin et al., 2002).

2.2. The Dirck Hartog Ridge

The DHR located in the centre of the PAP comprises a series of ridges of high bathymetric relief (in some locations >2000 m above surrounding ocean floor; Fig. 2a and b). Based on satellite gravity data and inferences from plate tectonic modelling, the DHR has previously been interpreted as an extinct mid-ocean ridge (Powell et al., 1988; Gibbons et al., 2012; Williams et al., 2013), or a pseudofault (Mihut, 1997; Mihut and Müller, 1998; Fig. 2c) but could possibly be a seamount chain associated with the Kerguelen plume. Interpretations of the DHR as a pseudofault were based on available magnetic anomalies (M0–M9) in the East PAP and an absence of conjugate anomalies in the west (Mihut, 1997; Fig. 2c). The type of pseudofault in this scenario develops as a result of a ridge jump forming an extinct ridge sub-parallel to

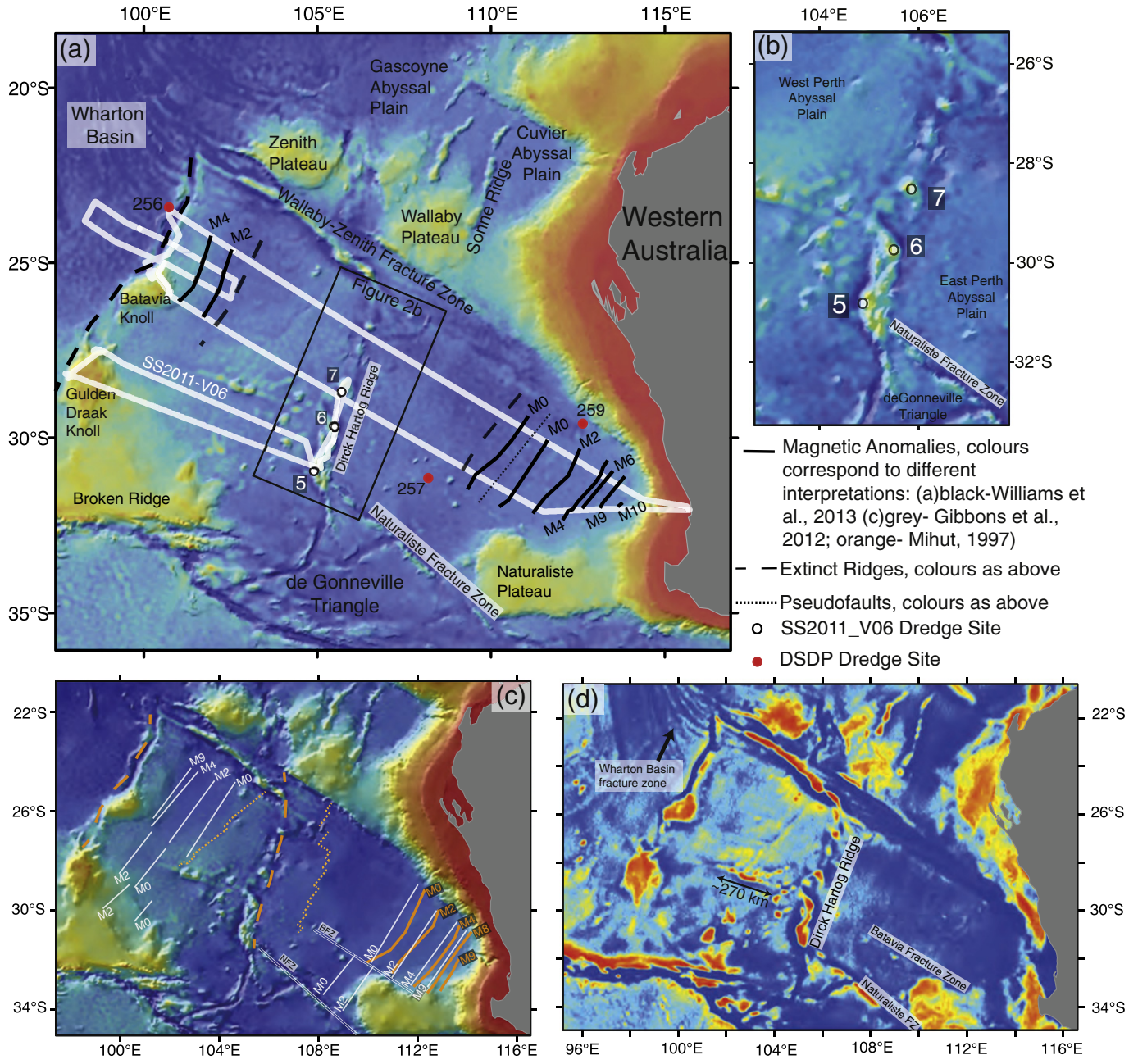

Fig. 2. (a) Bathymetric map of the Perth Abyssal Plain, showing existing data and interpretations: red dots are DSDP sites, dashed black lines are pseudofaults, dotted black lines are extinct ridges, solid black lines are interpreted magnetic anomalies (from Williams et al., 2013). Data from voyage SS2011_V06: White lines are ship tracks; numbered sites (5, 6, and 7) on Dirck Hartog Ridge are locations of mafic igneous dredges. (b) Close up of the bathymetry of the Dirck Hartog Ridge showing SS2011_V06 dredge locations. (c) Previous interpretations of the Perth Abyssal Plain: Mihut (1997) in orange, Gibbons et al. (2012) in white; solid black lines are magnetic anomalies, dashed black lines are pseudofaults, dotted black lines are extinct ridges. Double white lines are Batavia Fracture Zone (BFZ) and Naturaliste Fracture Zone (NFZ). (d) Gravity map of the Perth Abyssal Plain (Sandwell and Smith, 2009) showing distinctive bending fracture zones in the Wharton Basin and unusual seafloor morphology in the West PAP and the Batavia and Naturaliste Fracture Zones labelled (see Sections 4.1 and 5.3).

magnetic anomalies, rather than by ridge propagation (which usually forms pseudofaults oblique to magnetic anomalies). In the former, the ridge axis undergoes rapid and complete relocation, often due to weakening of oceanic crust by a mantle plume, to an entirely new location parallel to the original ridge axis, in a similar manner to that proposed for microcontinent formation (Müller et al., 2001). As a result, newly forming oceanic crust is juxtaposed next to older oceanic crust—bounded by a pseudofault. Mihut (1997) suggests the presence of two extinct ridges and one pseudofault, the DHR, created by multiple ridge jumps during the evolution of the PAP (Fig. 2c). More recently, Gibbons et al. (2012) synthesised a conjugate series of magnetic anomalies in the West PAP suggesting the DHR represents an extinct ridge that propagated from the north to south during the separation of India and Australia (as first suggested by Powell et al., 1988; Fig. 2c). The most recent interpretation of magnetic anomalies in the PAP (Williams et al., 2013) uses geophysical data collected on the SS2011_V06, revealing the conjugate Mesozoic anomalies in the West PAP adjacent to the Batavia and Gulden Draak knolls (Fig. 2a). Williams et al. (2013) observe that the DHR resembles neither a pseudofault nor a typical mid-ocean ridge and suggest that successive volcanism and/or tectonic events may have influenced the morphology of the DHR.

Immediately west of the PAP, sediment overlying basement (DSDP Site 256: Fig. 2a) provide minimum ages of the ocean crust in the adjacent Wharton Basin to be ~100 ± 1 Ma (Davies et al., 1974). In addition, recent $^{40}Ar/^{39}Ar$ dating of feldspar constrain the age of gabbro from the southern DHR (Site 5) to 102.3 ± 1.5 Ma (Whittaker et al., in review). These geological results, together with magnetic anomaly interpretations from Williams et al. (2013), strongly support interpretation of the DHR as an extinct mid-ocean ridge where spreading ceased between 101 and 104 Ma (Whittaker et al., in review). However, the evolution of the PAP from M0 (121 Ma) and the tectonic processes during the final stages of spreading in the PAP leading to the anomalous bathymetric expression of the DHR have not previously been explored.

3. Materials, methods, and data

3.1. Gravity and bathymetry

We use new bathymetric swath data collected in 2011 on the *R/V Southern Surveyor* (SS2011_V06) to characterise the DHR and CQZ ocean floor in the PAP. New multibeam bathymetry was acquired across the PAP perpendicular to the orientation of the DHR and magnetic anomalies (Fig. 2a), using the on board Simrad EM300 Multibeam Echo Sounder. Transits across the PAP from previous voyages (*R/V Melville*: BMRG06MV—1996 and SOJN04MV—1997, both collected using the Sea Beam 2000 Multibeam Echosounder) supported the 2011 PAP data set in the analysis of the DHR and PAP ocean floor. To determine zones of "rougher" and "smoother" ocean floor and characterise the morphology of the DHR and CQZ ocean floor we computed the slope, where the gradient, or rate of change in vertical units (z) is measured relative to neighbouring horizontal cells (x,y). Slope is expressed as a percentage, 0 = flat surface, and increases with verticality. Transverse (~E-W) profiles across the DHR were generated and compared to another previously identified fossil ridges of various ages around the world (the West Somali Extinct Ridge, the Osbourn Trough, the Phoenix Ridge, the Tasman Ridge) and a segment of an active mid-ocean ridge with a slow spreading rate similar to the rate calculated for the DHR (48.7 mm/yr full, the Central Indian Ridge; Small, 1989).

3.2. Sampling

Igneous samples were dredged from three sites on the DHR (SS2011_V06), dredge sites 5, 6, and 7, ranging from 2300 m to 3800 m water depth (Fig. 2a and b, Table 1). Representative sections of the whole rock, least affected by post-magmatic alteration, were selected for analysis (Table 2). Thin sections were observed under an Olympus BH2 polarising petrographic microscope.

3.3. Major and trace element abundance

Ten whole rock samples (4 gabbroic, 6 basaltic) were analysed for major and trace elements at Australian Laboratory Services Pty. Ltd. (ALS) in 2013 (ME-XRF26, ME-MS81, ME-4ACD81), using PANanalytical – Axios Max X-Ray Fluorescence (XRF) Spectrometer. Perkin Elmer SCIEX Elan 9000 Inductively Coupled Plasma - Mass Spectrometer (ICP-MS) was used to analyse the following resistive, minor and rare earth elements (REE): Ba, Ce, Cr, Cs, Dy, Er, Eu Ga, Gd, Hf, Ho La, Lu, Nb, Nd, Pr, Rb, Sm, Sn, Sr, Ta, Tb, Th, Ti, Tm, U, V, W, Y, Yb, and Zr, and volatile gold-related trace elements: As, Bi, Hg, Sb, Se, and Te. Agilent Technologies 700 Series Inductively Coupled Plasma-Atomic Emissions Spectrometer (ICP-AES) analysed base metals: Ag, Cd, Co, Cu, Li, Mo, Ni, Pb, Sc, and Zn.

In 2015, major and trace element abundances were analysed in 16 additional samples (including 5 duplicates from the original data set; DR5-56, DR6-6, DR7-2, DR7-4, DR7-5), using PANanalytical – Axios Max XRF Spectrometer at the University of Tasmania. Trace element composition was then analysed at the School of Earth Sciences, University of Melbourne, on an Agilent 7700x ICP-MS.

The analytical laboratories used in this study follow QA/QC practises that include multiple analyses of Certified Reference Materials (see Supplementary Material 1) and duplicates to monitor precision and accuracy when analysing unknown samples. For full details regarding machine conditions and methodologies, and the results of the duplicate samples compared with the original geochemical analyses see Supplementary Material (Fig. 1 and Table 1). Five samples were tested twice in different laboratories. These duplicates (DR5-56, DR6-6, DR7-2, DR7-4, DR75) were plotted on compositional diagrams to observe any inter-laboratory variation (Supplementary Fig. 1).

Table 1
Coordinates and depth ranges for dredges 5, 6, and 7 on the DHR from *SS2011_V06*.

Dredge	Start latitude	Start longitude	Start depth (m)	End latitude	End longitude	End depth
5	−30°48.458	104°52.414	3800	−30°47.240	104°53.410	2840
6	−29°41.828	105°31.358	3345	−29°42.990	105°29.871	2680
7	−28°29.900	105°50.542	2700	−28°30.463	105°49.927	2300

4. Results

Bathymetric swath data allow us to describe in detail features on the ocean floor in the PAP, which may help to constrain the spreading history during the CQZ where magnetic reversals cannot provide such information. Geological data from dredges enable us to ground truth geophysical data and accurately characterise the DHR in the context of seafloor spreading and mantle plume upwelling.

4.1. The Dirck Hartog Ridge and abyssal seafloor morphology

We present the first analyses of bathymetric swath from the PAP used to examine the DHR and abyssal seafloor morphology. The DHR defines the boundary between the East and the West PAP, rising up to ~2 km above the surrounding ocean floor and extends over 600 km in an NNE–SSW orientation (~018°E; Fig. 2b). Well-documented magnetic anomalies in the East PAP (Veevers et al., 1991; Mihut, 1997; Gibbons et al., 2013) trend NE–SW (~033–036°E) and are roughly perpendicular to the NW–SE trending Wallaby-Zenith Fracture Zone (bearing 125°E; Fig. 2a). Interestingly, the recently identified conjugate anomalies in the West PAP (Williams et al., 2013) show a trend closer to NNE (015–018°E) and are offset relative to the eastern magnetic anomalies by between 15° and 18°. The DHR orientation is sub-parallel to the West PAP M-series anomalies and thus also oblique to the trend of the interpreted M-series magnetic anomalies in the East PAP (Fig. 2a).

The relief across the entire DHR is highly irregular at the surface and has distinctive positive gravity anomalies (Fig. 2d). The ridge is asymmetric about the axis with deep troughs on the SW and NE margins and relatively shallow dipping NW and SE slopes. The southern portion of the DHR is characterised by a wide ridge (~50 km across at its widest point) 250 km in length, and 2800 m water depth at its shallowest point (Fig. 2b). The southernmost DHR meets the Naturaliste Fracture Zone at 31°S, 105°E. At this point, the eastern flank has a relatively low gradient with a more prominent slope and trough or moat around the western flank, with a strong negative gravity anomaly (Fig. 2d). Dredges from this part of the DHR sampled outcropping cumulate gabbro close to the ridge crest (Site 5). Gabbros recovered from the abyssal sea floor are important for understanding spreading mechanisms at mid-oceanic ridges, as exhumation of the lower crust often occurs during slower spreading (Cannat, 1993), with an intermediate magma supply (Tucholke et al., 2008). Gabbros from Site 5 not only provide information about spreading history of the PAP, but the location of these samples—at the crest of the southern DHR, may also provide evidence for tectonic uplift and/or faulting during or after ridge cessation. The

Table 2
Petrographic summary of basaltic/doleritic samples recovered from Sites 5, 6 and 7 on the DHR.

Sample number	Rock texture (hand specimen)	Petrographic description	Vesicles, veins, and fracturing	Secondary alteration
Site 5 (Dolerite)	No macroscopic variation in grain size, fine-grained but visible crystals. Considerable yellow discolouration in otherwise gray fine-grained but visible crystals	~1 mm long tabular euhedral grains of plagioclase with no preferred orientation. Plagioclase laths ~0.5—have rough irregular with cuspate indentations. Some display concentric zoning (possibly albite growth). Widespread chlorite fills microfractures, and epidote disseminated throughout Fig. 4a). High proportion of opaque minerals as well as epidote, chlorite, and prehnite. This sample is suspected to be a primary phase of spilitisation.	No vesicles. Some minor chlorite vein random network present.	Some discolouration on exposed surfaces, and secondary alteration minerals chlorite and epidote (Fig. 4b). Widespread yellow-brown alteration throughout.
Site 6 (Alkaline Basalt)	Reddish brown-gray aphanitic groundmass. Very altered in appearance.	This sample is largely made up of a yellowish dark brown alteration mineral smectite (Fig. 4d). Some acicular plagioclase present (<0.5 mm in length). Vesicles contain multiple fluid phases in chlorite infill. Relict pyroxene pseudomorphs are evidence of a basaltic origin.	Microscopic vesicles filled with multiple fluid rims (Fig. 4d)	Almost all original basaltic texture has been destroyed by hydrothermal fluid alteration in an evolving fluid rock system (Fig. 4d)
Site 7 (Alkaline Basalt)	Vesicles highly abundant suggestive of shallow eruption. Dark gray aphanitic groundmass.	Preferential orientations of thin secondary oxides reflect crystallographic control during breakdown of primary mafic minerals. Plagioclase grains occur as broken fractured laths, frequently with black micro granular strip running long edge parallel although the centre of the grain. No primary igneous texture is visible. At ×5 magnification appears as networks of radiating needles (Fig. 4c).	Vesicles are ~15–20% of total rock proportion, highly variable vesicle size (2–9 mm diameter). Selected samples have chlorite filled vesicles; others contain no chlorite infill but contain red-brown clay alteration minerals around vesicle rims.	Multiple fluid phases have overprinted original rock texture. Smectite alteration and red-brown discolouration throughout.

morphology and geological samples from this segment of the DHR are important for understanding the tectonic mechanisms involved in the formation of this ridge (discussed in Sections 5.1 and 5.3).

Northward, the DHR deepens to ~3900 m to form a saddle structure between two higher relief segments. This saddle is cut by a deep channel of an NE–SW orientation, which bends to form a steep scarp on the northeast flank of the DHR towards Dredge Site 6. The western flank, near Site 6, has a much smoother lower gradient slope than in the south. The northernmost dredge site (7) is located on a completely bathymetrically distinct segment, separated from the nearest ridge to the south by ~90 km of deeper ocean floor. This northern segment of the DHR resembles an elongate asymmetric mound, is similar in orientation to the southern ridge, with a steep south-eastern scarp and a shallowly dipping north-western slope. The mound is no more than 30 km across and is the shallowest point on the DHR, at a depth of ~2200 m (Fig. 2b). Alkali basalts were dredged from the eastern flank of this part of the DHR.

Abyssal fabric is an expression of the mechanisms of seafloor spreading processes that formed it (Goff et al., 1997, 2004). Seafloor fabric can reveal information about paleo-seafloor spreading processes including, evidence for acceleration/deceleration in spreading rate, and the presence and nature of fracture zones, pseudofaults and extinct ridges (Carbotte and Macdonald, 1994; Smith, 1998). Analysis of bathymetry in deep ocean basins and across abyssal plains can be used to identify features of the seafloor as the blanketing effect of sediments is expected to be minimal. In particular, the PAP shows minimal sediment cover according to total sediment thickness as calculated by the age and tectonic history of the oceanic crust, structural trends in the basement, and the possible origins of sediment to the basin (Divins, 2003). Deep Sea Drilling Programs with cores in the East PAP also support a relatively thin layer of sediments in this region, with depth to basement no more than 300 m at both Sites 257 and 259 (Deep Sea Drilling Project, 1989). We analyse and compare the morphology of the East and West abyssal plains to help constrain the spreading history of the PAP. Older seafloor generated during the Early Cretaceous in both the East and West PAP (where M-Series anomalies identified spreading to be 35 mm/yr) is relatively smooth and uniform, compared to the younger CQZ seafloor towards the centre of the PAP that exhibits more variable and rougher surface morphologies (Fig. 3a and b). Swath bathymetry profiles (SS2011_V06 and SOJN04MV) show a transition from relatively smooth abyssal hill fabric, towards rougher and more irregular ocean floor and increasing rugosity towards the DHR on both the East and West flank of the PAP (Fig. 3a–d). This region of rough ocean floor extends ~300 km either side of the DHR and the apparent symmetry suggests it is related to tectonic processes and formed as a result of slowing seafloor spreading rates, which are commonly associated with rougher basement morphology (Malinverno, 1991; Whittaker et al., 2008).

Although there is a transition from smooth to rough on both flanks, the eastern and western conjugate flanks of the PAP have very distinct morphologies. The West PAP is appreciably rougher with more varied bathymetric relief across the entire flank in the form of seamounts, scarps, positive gravity anomalies and in some regions is up to ~400 m shallower than its eastern conjugate (Fig. 2a and d). If such distinctive irregularities in seafloor morphology were attributed only to spreading rates, we would expect to see similar bathymetric features on both flanks of the PAP. However, the eastern conjugate has substantially less variable bathymetric relief and a more regular gravity signature (Fig. 2d). In general, observations from bathymetric swath show that the East PAP is characterised by relatively smooth abyssal seafloor between 5000 and 5500 m water depths. Approaching the DHR, the abyssal fabric becomes more irregular and the abyssal hills become more apparent in the SOJN04MV swath profile within 300 km of the DHR (Fig. 3c). The gravity signature is regular across the East PAP with the most prominent positive gravity anomalies ~100 km east of dredge Sites 6 and 7. Towards the southern East PAP adjacent to the Naturaliste Plateau, the ocean floor exhibits some elevated bathymetric relief and seamounts. Mesozoic magnetic anomalies M2 and M0 have been interpreted in this portion of ocean crust suggesting they are

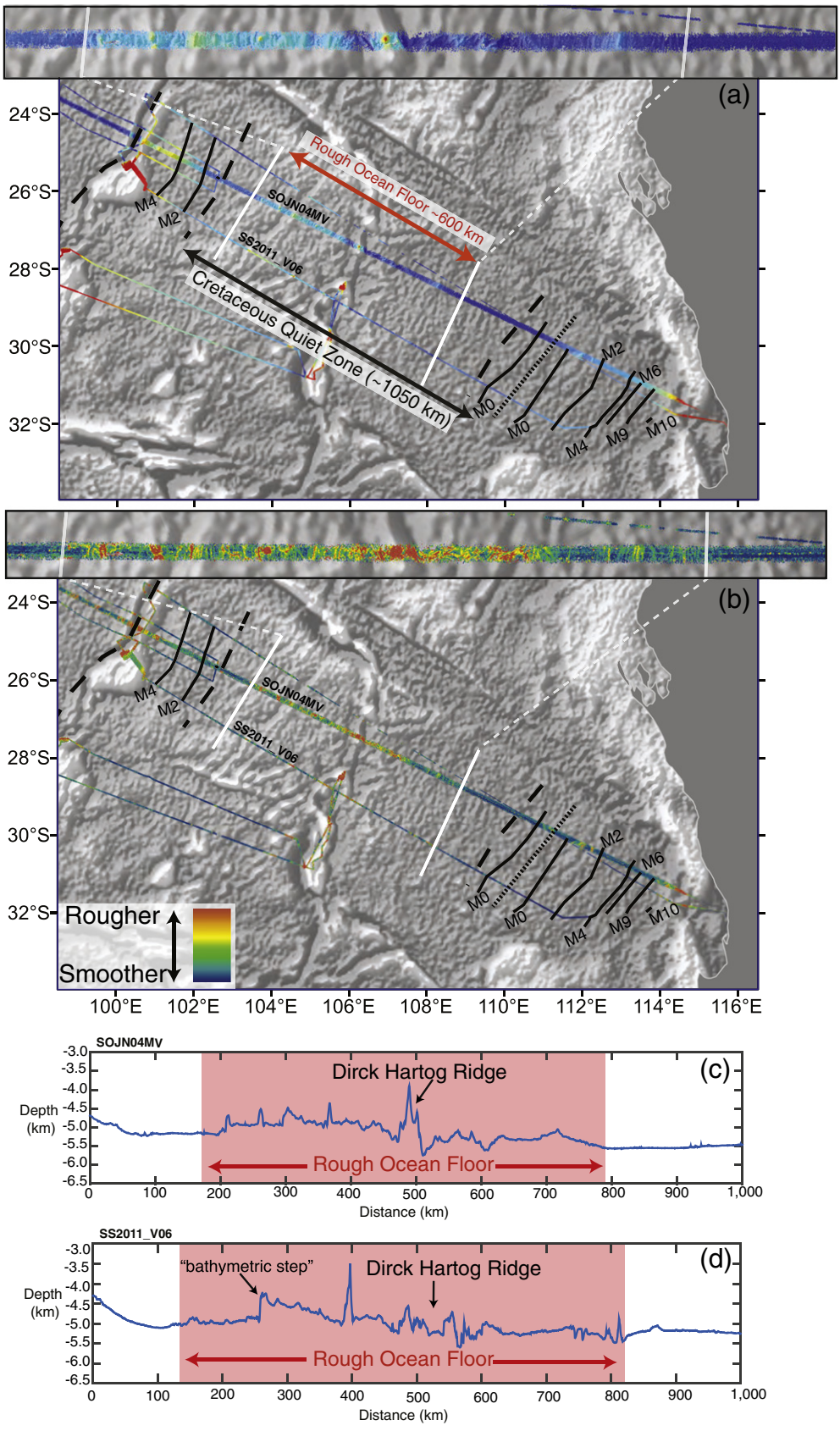

Fig. 3. (a) Gray scale gravity map with bathymetric swath profiles (coloured) traversing the Perth Abyssal Plain (SS2011_V06 on the R/V Sothern Surveyor in 2011 and the SOJN04MV transit on the R/V Melville in 1997). (b) Gray scale gravity map with slope analysis of the swath data, determined by ArcGIS, used to characterise the abyssal seafloor. Previously interpreted pseudofaults (dashed lines), extinct ridges (dotted lines) and labelled Mesozoic magnetic anomalies (solid black lines) are from Williams et al. (2013). (c) Profiles along swath line SOJN04MV and (d) SS2011_V06 with the identified region of rough ocean floor highlighted in red, and features referred to in the text; the Dirck Hartog Ridge and the "bathymetric step" are labelled.

continuations of Mesozoic anomalies in the East PAP, offset by the Batavia fracture zone, and formed during southern propagation of the mid-oceanic ridge between India and Australia.

A distinctive feature in the centre of the West PAP is an ENE–WSW trending elongate ridge ~270 km in length, ~100 km from the western flank of the DHR near Site 6 (Fig. 2d). The ridge is orthogonal to the DHR, shows a distinct positive gravity anomaly, and appears asymmetric about its axis, with a low gradient flank to the north and a steeper scarp to the south. Several bathymetric mounds on the northern flank radiate northwards and surround the ridge to the east and south with no apparent orientation. To the north of the ENE–WSW trending elongate ridge, an abrupt change in bathymetric elevation of ~500 m, herein referred to as a "bathymetric step," can be identified in the SS2011_V06 swath profile (Fig. 3d). Mihut (1997) interpreted this feature as an extinct mid-ocean ridge that was active during the CQZ (Fig. 2c). If this feature is an extinct ridge, then we would expect the pronounced change in elevation to be a linear feature that would continue northward; however, it is much less apparent in the northern SOJN04MV profile (Fig. 3c). The origins of the "bathymetric step" are not discussed in Gibbons et al. (2012), although Williams et al. (2013) refer to this feature as a major linear positive anomaly, oblique to magnetic anomalies but do not incorporate it into their model. The absence of magnetic anomaly M0 (121 Ma) in the West PAP, and a duplication of M0 in the East PAP suggests a portion of crust, adjacent to the "bathymetric step," is missing in the West PAP.

The marked differences in morphology of oceanic crust in the West PAP compared to the East PAP, as well as the anomalous morphology and skewed orientation of the DHR relative to magnetic anomalies contribute to an overall regional asymmetry in the PAP.

4.2. Petrographic results

Dredged material from the DHR included both intrusive and extrusive mafic igneous rocks, confirming the ridge's oceanic nature. The basalt (Sites 6 and 7) and the dolerite (Site 5) derived from the DHR are all dark gray-black aphanitic (basaltic) to fine-grained (doleritic) volcanic to sub-volcanic rocks with visible marine alteration in the form of yellow-brown discolouration around vesicles, veins, and fractures (see Table 2 for petrographic summary). To the north (Site 7), basalts have high proportions (~35%) of vesicles, no larger than 0.9 cm diameter, the majority of which are filled with secondary calcite. Basalts derived from Sites 5 and 6 (DR5-8, DR5-60, DR6-6) on the DHR contain a noteworthy calcite vein network and fewer vesicles than Site 7, most of which are <1 mm diameter.

In thin section, all basaltic samples show variable degrees of hydrothermal alteration, and in some cases low-grade metamorphism-spilitisation (Fig. 4a–d). Spilitisation is characterised by needle-like radiating textures in glassy domains of some samples (DR6-6, DR7-2, DR7-4, DR7-5) and the presence of deuteritic alteration minerals: epidote, smectitie, chlorite, calcite, zeolites, and prehnite.

Gabbroic samples were dredged at Site 5 (DR5-3, DR5-10, DR5-32, DR5-60) in addition to the dolerite samples. These samples contain coarse plagioclase with variable proportions of pyroxene (Fig. 5; see Table 3 for full petrographic summary). The early crystallising mineral assemblage (i.e., pyroxene and plagioclase) and high plagioclase proportions in some samples is typical of a cumulate setting (Natland and Dick, 2001). The lack of obvious trapped melt or crystal zoning suggests gabbros from Site 5 are adcumulates. Exsolution textures observed in all gabbroic samples are indicative of a prolonged cooling period (Fig. 5a

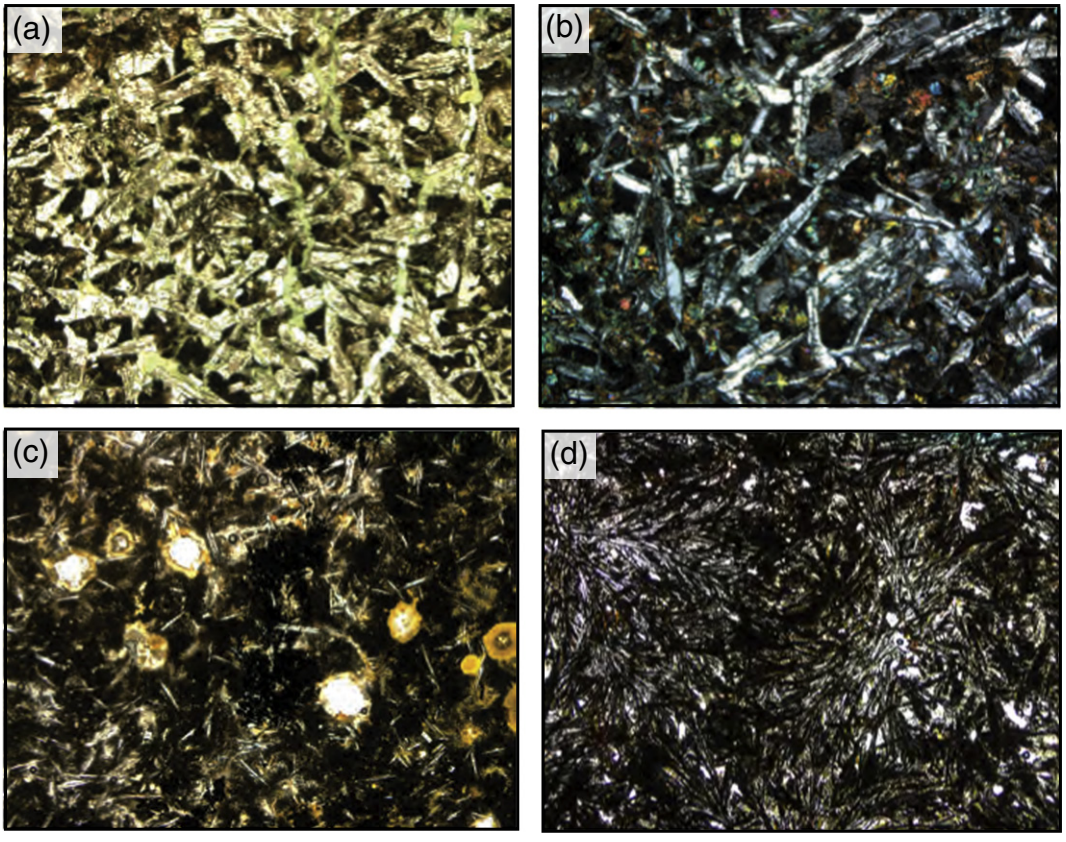

Fig. 4. (a). Photomicrograph of basaltic sample from Site 5 (DR5-8) in plane polarised light, field of view 4 mm. Elongate plagioclase laths randomly oriented and chlorite alteration (green) and smectite (dull brown discolouration) visible throughout. (b) Photomicrograph of basaltic sample from Site 5 (DR5-8) in crossed polarised light, field of view 4 mm. Epidote minerals visible as highly birefringent round grains. (c) Photomicrograph of basaltic sample from Site 6 (DR6-6) in plane polarised light, field of view 4 mm. Microscopic vesicles filled with multiple fluid rims suggest multiple phases of hydrothermal fluid percolated this rock causing extensive alteration and destruction of primary igneous texture. (d) Photomicrograph of basaltic sample from Site 7 (DR7-5) in plane polarised light, field of view 4 mm. Needle-like radiating textures (spilitisation) and abundant smectite alteration and red-brown discolouration throughout.

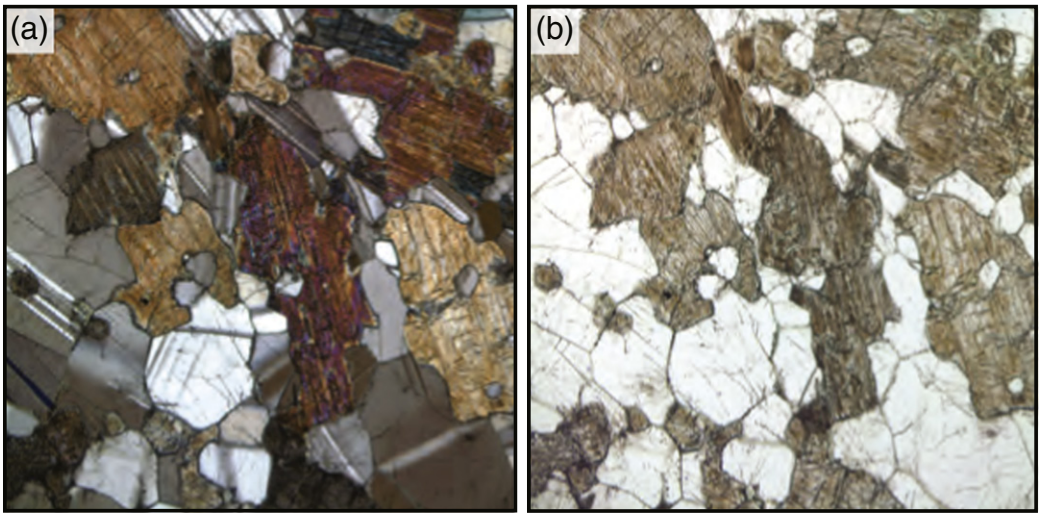

Fig. 5. Photomicrograph of gabbroic sample (DR5-56) from Site 5 in crossed polarised light (a) and plane polarised light (b), width of field of view 4 mm. This sample is predominantly made up of plagioclase (colourless mineral in plane polarised light, polysynthetic twinning in crossed polarised light) and pyroxene (brown high relief mineral in plane polarised light) with strong exsolution lamellae of orthopyroxene/clinopyroxene (stripy texture) indicative of slow cooling.

and b). No obvious compositional layering is visible in these samples; however, layering of gabbroic samples is less common in gabbros outcropping on the ocean floor than observed in ophiolites (Karson, 1998). Ophiolite studies have long suggested that gabbros and cumulate gabbros, such as those gabbros dredged from Site 5, are typical of lower oceanic crust (Layer 3B; Peterson et al., 1974). Drilling and sampling of the ocean floor allows documentation of the regions where lower crustal gabbros are outcropping at the surface, such as ODP Site 735, Leg 118 that drilled a fracture zone on the South West Indian Ridge (Robinson et al., 1988; Dick et al., 1993; Karson, 1998). These studies reveal important information about the structure of the oceanic lithosphere, as well as the context in which faulting mechanisms that are responsible for core complex formation. In many areas, including the South West Indian Ridge, lower crust is exhumed by detachment faulting in periods of slower spreading (Dick et al., 1993; Cannat et al., 2006). Secondary alteration minerals are also present in some samples suggesting hydrothermal fluid percolation through fractures.

4.3. Geochemical results

All basaltic samples show some degree of hydrothermal alteration in hand specimen, thin section and in major element composition (LOI up to 16 wt. %; Table 4). As a result, sample classification and analysis largely made use of immobile trace elements.

Sub-alkaline dolerite samples from Site 5 have incompatible element concentrations an order of magnitude lower than the alkaline basaltic samples (from Sites 6 and 7) and are most similar to Depleted Mid-Ocean Ridge Basalt (DMORB, as defined by Gale et al., 2013; Fig. 7a). High levels of mobile U and enrichment in Rb, Ba, and Th relative to DMORB are observed in samples from Site 5 and are attributed to post-magmatic hydrothermal alteration processes rather than a characteristic of the magma source.

Gabbroic samples from Site 5 are depleted in TiO_2, Fe_2O_3, and P_2O_5 and enriched in CaO, Al_2O_3, and MgO compared to the dolerites from the same location. Overall, there are significantly lower trace element concentrations in all gabbroic samples, compared to the basaltic samples, in some cases close to the limits of detection (Fig. 6b). The gabbroic samples also have higher concentrations of compatible elements (Cr, Ni) compared to the basaltic samples, which makes up the early forming crystallising assemblage. Three of the four gabbroic samples show Sr enrichments and all samples show a subtle Eu enrichment, indicative of plagioclase accumulation (Hart et al., 1999). Relatively low concentrations of Y and Ti is consistent with an adcumulate origin for these gabbros with minimal trapped intercumulus melt (Beccaluva et al., 1977). Enrichment of U and K in these samples is most likely attributed to secondary alteration as neither plagioclase nor pyroxene grains contain abundant U or K (Table 4).

Overall, subvolcanic samples from Site 5 have the following geochemical attributes: (1) they are light rare earth element depleted

Table 3
Petrographic summary of gabbroic samples recovered from Sites 5 on the DHR.

Sample number	Rock texture (hand specimen)	Petrographic description	Vesicles, veins, and fracturing	Secondary alteration
DR5-3	Coarse-grained holocrystalline, dominated by well defined white-gray plagioclase with some subhedral dark green pyroxene	Irregular subhedral grains of plagioclase with relatively low relief more prominent compared to anhedral pyroxene. Exsolution texture in pyroxene with fractured clinopyroxene dominating (Fig. 5b)	Abundant micro-fractures predominately in plagioclase	Highly altered and fractured with sparse opaque minerals
DR5-10	Dominated by gray plagioclase with ~5% pyroxene	Sample contains >70% plagioclase with some anhedral interstitial pyroxene	Abundant microfractures predominately in plagioclase	Difficult to distinguish any alteration minerals due to intense fracturing
DR5-32	High proportion of ~1 cm pyroxene grains (~40–50%) and white-gray plagioclase	High proportion of large euhedral pyroxene with exsolution textures. Plagioclase also present though extremely fractured (Fig. 5a)	Abundant microfractures predominately in plagioclase	Difficult to distinguish any alteration minerals due to intense fracturing
DR5-56	Dark green-gray colour with opalescent character, fine-grained (<3 mm) interlocking grains	Sample contains irregular subhedral plagioclase grains with anhedral brown-green high relief fractured pyroxene (Fig. 5a)	Some minor fracture networks in hand specimen	Some discolouration adjacent to fractures

Table 4
Major (wt.%) and trace (ppm) element data for samples from the DHR, *SS2011_V06*. Asterisk denotes those samples analysed at the ALS (2013). All other samples were analysed at the University of Tasmania (XRF) and the University of Melbourne (ICP-MS) in 2015 (see Section 3.3 for details).

Major Elements	DR5-8*	DR5-61*	DR6-1	DR6-10	DR6-11	DR6-2	DR6-4	DR6-6	DR6-7	DR6-8	DR6-9	DR7-1B	DR7-2	DR7-3	DR7-4	DR7-5	DR6-5	DR5-3*	DR5-10*	DR5-32*	DR5-56
Rock Type	Dolerite	Dolerite	Basalt	Basalt	Basalt	Basalt	Basalt	Basalt	Basalt	Basalt	Basalt	Basalt	Basalt	Basalt	Basalt	Basalt	Basalt	Gabbro	Gabbro	Gabbro	Gabbro
SiO_2	49.00	48.20	43.62	42.97	43.76	44.74	44.82	46.20	43.55	42.92	45.49	46.33	34.07	46.38	46.15	50.16		46.80	46.20	48.90	49.60
TiO_2	1.05	1.33	1.44	1.31	1.44	1.42	1.47	1.36	1.52	1.36	1.18	2.49	2.00	2.48	2.58	2.95		0.11	0.05	0.10	0.17
Al_2O_3	14.75	16.20	15.39	15.83	15.67	15.56	16.07	15.36	16.14	14.97	14.73	14.55	11.22	14.79	14.74	16.72		19.80	28.40	19.20	17.45
Fe_2O_3	12.27	14.14	7.67	10.65	10.25	11.36	10.78	9.59	7.51	8.31	9.90	8.08	6.31	7.89	8.49	8.95		4.83	2.16	3.59	5.79
MnO	0.2	0.2	0.1	0.0	0.2	0.3	0.1	0.2	0.1	0.1	0.2	0.1	0.1	0.1	0.1	0.1		0.08	0.03	0.07	0.10
MgO	7.21	5.62	3.41	2.35	2.41	3.13	2.71	5.42	1.62	3.34	5.67	5.46	1.14	5.14	3.77	1.55		10.35	4.24	9.48	9.35
CaO	11.20	8.62	13.35	11.45	10.44	9.87	9.40	10.65	12.59	12.49	12.98	8.19	21.62	8.74	8.89	5.61		12.00	14.15	13.90	14.60
K_2O	2.11	2.47	2.19	2.41	2.34	2.43	2.51	2.48	2.36	2.25	2.13	3.81	2.75	3.90	3.96	4.11		1.07	1.94	1.09	1.38
Na_2O	0.11	0.35	2.71	2.61	2.48	2.08	2.02	1.00	3.37	2.46	0.89	2.52	3.24	2.59	2.98	4.84		1.32	0.26	0.98	0.24
P_2O_5	0.08	0.14	4.53	4.08	2.54	2.65	2.35	1.54	5.24	4.35	0.40	0.99	1.25	1.03	1.13	2.02		0.01	0.01	0.02	0.01
LOI	1.76	2.62	5.50	6.12	8.40	6.26	7.39	6.00	5.89	6.77	6.39	7.34	16.12	7.30	6.71	2.78		3.32	2.30	2.52	1.60
Total	99.97	100.15	99.88	99.83	99.89	99.82	99.62	99.77	99.86	99.32	99.91	99.85	99.81	100.32	99.52	99.76		99.99	99.84	100.15	100.55
Mg#	0.56	0.47	0.49	0.33	0.34	0.38	0.36	0.55	0.32	0.47	0.56	0.60	0.59	0.29	0.49	0.28		0.83	0.81	0.85	0.79
Trace Elements																					
Cr	220	130	537	401	446	523	543	482	442	492	578	162	156	138	159	179	590	960	130	1040	780
Co	50	44	21	18	35	56	37	42	20	22	64	31	31	24	30	33	24	39	19	30	34
Ni	91	76	90	58	129	166	131	146	66	104	179	168	164	94	146	138	96	199	114	180	173
Rb	2.7	7.4	32.6	43.1	49.6	49.7	44.9	15.9	43.3	33.1	16.6	46.5	51.7	51.1	52.1	64.7	18.6	11.6	2.6	8.7	2.3
Sr	92.8	88.6	353.2	295.2	296.9	326.5	300.3	324.7	368.2	543.6	178.4	637.2	658.5	661.4	667.6	772.2	327.5	53.9	132.6	49.5	60.6
Cs	0.22	0.47	1.31	1.79	1.77	2.08	1.68	0.66	1.90	1.19	0.69	0.96	0.95	0.58	1.23	0.97	0.73	0.18	0.05	0.24	0.07
Ba	40	36	170	137	180	780	198	890	261	4584	106	604	673	598	635	722	1130	89	18	15	6
Sc	46	50	37	37	40	38	38	40	39	37	36	14	16	14	15	16	36	27	3	24	39
V	316	345	171	130	96	136	97	207	128	163	203	82	93	116	99	151	200	57	18	47	152
Nb	2.0	1.7	21.1	15.9	21.7	20.8	21.8	21.4	22.5	21.1	14.6	54.4	60.9	52.9	54.5	64.2	19.9	0.5	0.2	0.2	0.035
Zr	65	71	105.8	92.3	108.2	106.2	109.0	108.6	114.2	105.7	81.2	383.4	426.2	359.5	387.3	420.5	101.6	10	2	4	2.5
Hf	1.8	2.1	2.69	2.43	2.76	2.68	2.77	2.73	2.93	2.66	2.06	8.15	9.11	7.78	8.21	9.53	2.55	0.2	0.2	0.2	0.11
Th	0.36	0.61	1.86	1.38	1.94	1.82	1.92	1.91	2.00	1.88	1.14	2.69	2.99	2.59	2.67	3.15	1.79	0.41	0.05	0.06	0.005
U	0.8	0.9	1.45	1.09	0.89	0.89	0.92	0.88	1.58	1.58	0.32	0.88	0.97	1.06	0.95	1.39	0.75	2.51	0.11	0.35	0.029
Y	26.87	30.29	79.84	53.48	79.52	74.81	65.95	27.63	40.82	38.97	24.81	25.64	28.69	24.96	25.44	45.26	32.55	5.90	0.61	3.08	5.17
La	3.6	3.3	59.8	33.0	64.4	61.3	49.2	17.3	32.6	27.9	12.3	40.7	45.1	39.0	40.4	54.8	20.5	2.9	0.5	0.5	0.16
Ce	9.5	8.9	32.3	28.4	33.8	32.8	34.2	33.1	35.2	32.4	22.5	85.6	94.5	81.9	85.1	99.6	30.7	4.7	0.5	0.5	0.47
Pr	1.41	1.44	7.53	4.96	7.68	8.15	7.39	4.30	5.28	4.76	2.99	10.84	12.01	10.42	10.73	13.71	4.49	0.55	0.03	0.03	0.10
Nd	7.4	7.9	30.8	21.0	31.4	33.2	30.3	17.9	21.8	19.8	12.8	43.4	48.2	41.8	43.0	55.3	18.7	2.2	0.2	0.3	0.7
Sm	2.65	2.88	6.01	4.63	6.02	6.35	6.13	4.17	4.80	4.34	3.14	8.57	9.44	8.23	8.46	10.81	4.21	0.46	0.31	0.26	0.33
Eu	1.14	1.22	1.82	1.48	1.84	1.92	1.86	1.36	1.54	1.40	1.04	2.81	3.05	2.66	2.77	3.44	1.35	0.22	0.23	0.19	0.23
Gd	3.94	4.38	7.89	5.91	8.04	8.34	7.72	4.64	5.60	5.03	3.77	7.43	8.20	7.11	7.35	9.83	4.80	0.96	0.11	0.42	0.61
Tb	0.72	0.81	1.18	0.96	1.18	1.23	1.17	0.77	0.90	0.81	0.64	1.03	1.14	0.99	1.02	1.38	0.79	0.18	0.02	0.07	0.12
Dy	4.69	5.32	7.66	6.24	7.71	7.84	7.50	4.87	5.70	5.14	4.15	5.49	6.12	5.29	5.45	7.58	5.02	0.79	0.18	0.49	0.89
Ho	1.08	1.16	1.82	1.45	1.84	1.84	1.74	1.06	1.27	1.16	0.93	1.02	1.13	0.98	1.01	1.50	1.11	0.20	0.03	0.10	0.21
Er	3.35	3.69	5.32	4.23	5.32	5.25	4.97	2.99	3.61	3.32	2.68	2.56	2.82	2.45	2.53	3.88	3.20	0.56	0.12	0.32	0.61
Tm	0.53	0.55	0.76	0.62	0.76	0.75	0.72	0.44	0.53	0.49	0.40	0.35	0.38	0.33	0.34	0.53	0.47	0.12	0.03	0.06	0.09
Yb	2.88	3.41	4.67	3.88	4.65	4.65	4.43	2.83	3.35	3.09	2.57	2.07	2.26	1.97	2.05	3.18	3.03	0.48	0.17	0.34	0.60
Lu	0.50	0.50	0.74	0.60	0.73	0.71	0.68	0.42	0.51	0.48	0.39	0.29	0.32	0.28	0.29	0.46	0.46	0.12	0.02	0.05	0.09
Cu	170	224	61	72	78	119	89	97	69	73	98	26	34	30	36	85	81	234	58	78	94
Zn	104	170	156	150	142	176	164	176	166	156	167	101	169	132	149	171	132	67	34	43	46
Ti	6408	8188	8168	7803	8633	8051	8542	7805	9019	8264	6498	14,730	16,453	14,203	14,832	17,347	8487	682	307	615	966

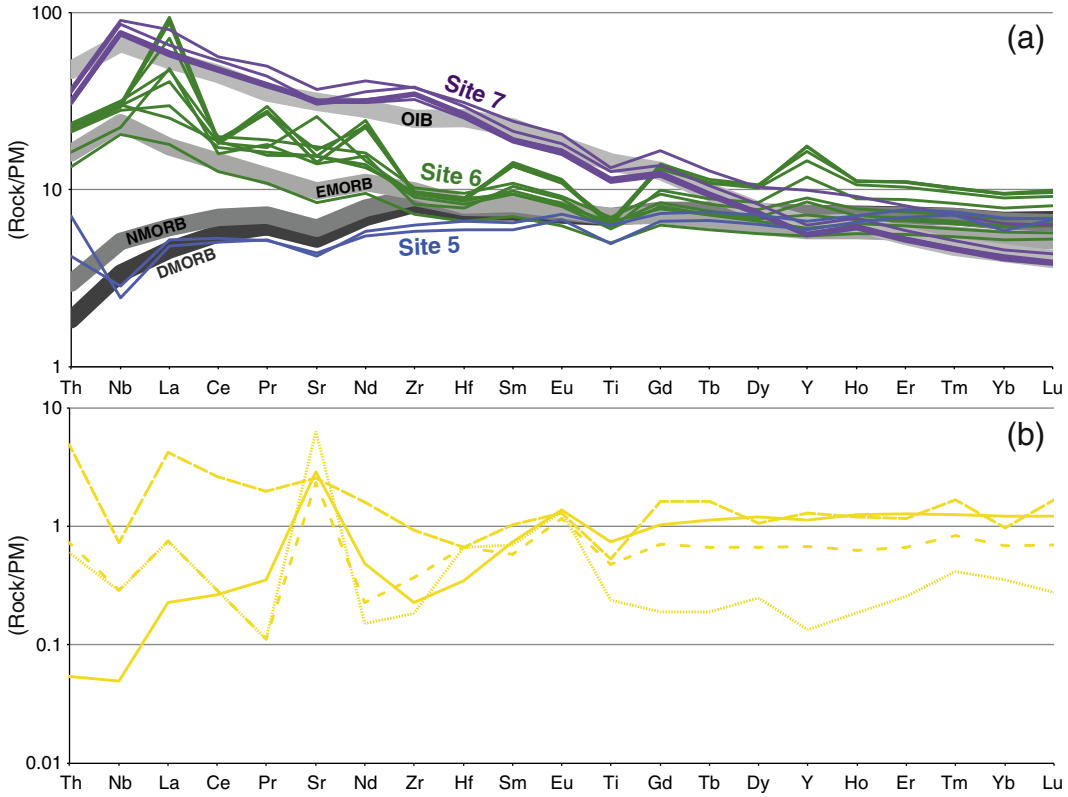

Fig. 6. (a) Multi element plot of the basaltic samples from the Dirck Hartog Ridge normalised to Primitive Mantle (PM, Sun and McDonough, 1989) Site 7 basalts (purple), Site 6 basalts (green), Site 5 dolerites (blue). Average trace composition of depleted mid-ocean ridge basalt (DMORB), normal MORB (NMORB), enriched MORB (EMORB) from Gale et al. (2013), and average ocean island basalt (OIB) trace composition from Sun and McDonough (1989). (b) Multi element plot of gabbroic samples from Site 5 on the DHR (yellow). All samples are normalised to Primitive Mantle (PM) abundances according to Sun and McDonough (1989).

(Fig. 7a), (2) relative Nb and La concentrations are most comparable to DMORB (Fig. 7b), (3) they have low $[Ce/Y]_N$ ratios (0.8–0.9; Fig. 7c), (4) $[Ti/Y]_N$ typical of divergent boundaries (NMORB/DMORB; Fig. 7d; Pearce and Norry, 1979), and (5) $[Sm/Yb]_N$ ~1 (Fig. 7e). Typically, a relative depletion in highly incompatible elements compared to Heavy Rare Earth Elements (HREE) is interpreted to be a result of adiabatic melting of a typical MORB source at a mid-ocean ridge setting (Shen and Forsyth, 1995; Pearce, 2008). Furthermore, concentrations of Zr, Y, and Nb from these Site 5 rocks overlap with basalts recovered from ODP Sites 257 and 259 in the West PAP, which are thought to represent typical Indian Ocean floor basalt (Fig. 7a; Davies and Luyendyk, 1974). They also show Light Rare Earth Element (LREE), High Field Strength Element (HSFE) and HREE concentrations similar to the average compositions of samples recovered along South East Indian Ridge between 70°E and 120°E (Gale et al., 2013; Fig. 7a–e). Samples from both the South East Indian Ridge and Site 5 on the DHR display low $[Zr/Y]_N$ and $[Ti/Y]_N$ ratios (where, the ratio ≤ 1), which is characteristic of divergent plate boundary volcanism or larger extents of melting of a source depleted in incompatible elements (Fig. 7a and d; Langmuir et al., 1992; Pearce and Norry, 1979).

Interestingly, there are similarities in $[Nb/La]_N$ and $[Th/Nb]_N$ between Site 5 and lavas from the Elan Bank, volcanic rocks from offshore Western Australian (Wallaby Plateau; Fig. 2a), and tholeiitic samples from the Naturaliste Plateau (Fig. 7b). The relative depletion of Nb versus Th in the Elan Bank samples is interpreted to derive from a fragment of continental crust, which was entrained in upwelling Kerguelen magmas (Ingle et al., 2002; Gaina et al., 2007). In the Naturaliste Plateau tholeiitic series, the Nb depletion is attributed to shallow contamination of continental lithosphere (Mahoney et al., 1995). The slight Nb trough in offshore Western Australia volcanics is attributed to either a plume source or to contamination of magmas by the thinning lithosphere (Dadd et al., 2015). For Site 5 dolerites on the DHR, it is most likely that the subtle Nb trough is inherent in the Indian Ocean MORB. Alternatively, the Nb trough results from the mixing of a relict of Gondwanan continental lithosphere with the asthenosphere similar to interpretations of samples from the Naturaliste Plateau.

On the other end of the spectrum, samples from Sites 7 (the northernmost site on the DHR; Fig. 2b) show relative enrichment of incompatible elements, HFSE, large-ion lithophile elements (LILE), LREE (compared to HREE), similar to average Ocean Island Basalt (OIB) as defined by Sun and McDonough (1989; Fig. 6a). They also have consistently higher values for selected HFSE and LREE (namely, Nb, La, Ce, Pr, Zr, and Hf and to lesser degree Sm and Ti) than the sub-alkaline dolerites (Site 5; Fig. 6a). Site 7 lavas are extremely enriched in incompatible elements, demonstrated by elevated abundance ratios $[Nb/Zr]_N$ (~2), $[Nb/Y]_N$ (10.3–11.6), $[Zr/Y]_N$ (5.1–5.9), $[Ti/Y]_N$ (1.8–2.1), and $[La/Sm]_N$ (3.4–3.7) (Fig. 7a, d, e) compared to Sites 5 and 6 on the DHR. Lavas highly enriched in LREE, HFSE, and LILE, with incompatible element concentrations comparable to average OIB, indicate that these lavas were derived from small degrees of partial melting of an incompatible element-enriched source. Elevated $[Sm/Yb]_N$ (~4) and $[Ce/Y]_N$ (8.5–9.2) ratios observed in Site 7 basalts suggest melting at a greater depth than those from Site 5 (Fig. 7c and e). More evolved lavas, such as those recovered from Site 7, are characteristic of the final phases of spreading at a dying ridge or of excess volcanism; as magma supply diminishes, magma chambers form in the crust and fractional crystallisation is a dominant magma process (Frey et al., 2000).

Volcanic rocks at Site 7 are much more enriched in incompatible elements when compared to volcanic products of the Kerguelen plume that was active around the time of PAP formation (Elan Bank, Central

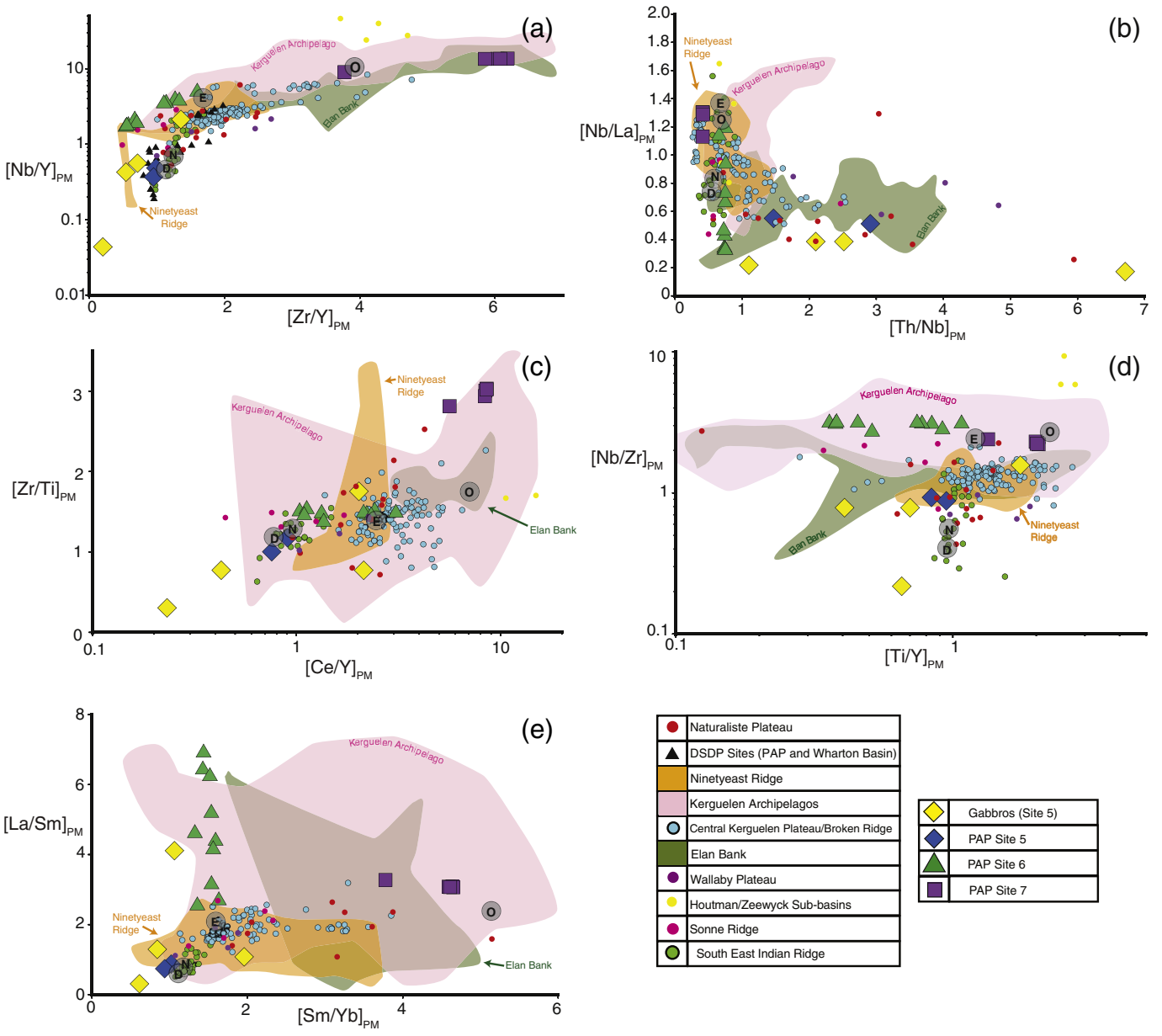

Fig. 7. Normalised trace ratio plots of samples from the Dirck Hartog Ridge compared to regional contemporaneous volcanism from the Naturaliste Plateau, DSDP Sites 256, 257 (Leg 26), 259 (Leg 27), the Ninetyeast Ridge (DSDP Sites: 214, 215, 216, 253, 254, 756, 757, 758), the Kerguelen Archipelago, the Central Kerguelen Plateau (OPD/DSDP Sites 1138 and 747) and Broken Ridge (Sites 1141/1142), the Elan Bank (Site 1137), Eastern Indian Ocean (Gale et al., 2013), and volcanic rocks from the Western Australian margin (Dadd et al., 2015). Data sources are in background data set—Supplementary Data 2. See Section 4.3 for description and Section 5.2 for interpretation. Average values for ocean island basalt (O; Sun and McDonough, 1989), enriched (E), normal (N), and depleted (D) mid-ocean ridge basalt (Gale et al., 2013). (a) $[Zr/Y]_{PM}$ vs. $[Nb/Y]_{PM}$. (b) $[Th/Nb]_{PM}$ vs. $[Nb/La]_{PM}$. (c) $[Ce/Y]_{PM}$ vs. $[Zr/Ti]_{PM}$. (d) $[Ti/Y]_{PM}$ vs. $[Nb/Zr]_{PM}$. (e) $[Sm/Yb]_{PM}$ vs. $[La/Sm]_{PM}$.

Kerguelen Plateau/Broken Ridge, and the Ninetyeast Ridge), although these samples do have geochemical similarities with more recent (~29 Ma) volcanic rocks from the Kerguelen Archipelago (Fig. 7a–e). The alkaline Kerguelen Archipelago volcanism is suggested to be a product of highly fractionated magmas either during low magma supply, increased lithospheric thickness, hotspot migration, or a decrease in magma flux (Nicolaysen et al., 2000; Frey et al., 2002; Xu et al., 2007). A similar geochemical signature is found in basanite samples from volcanic cones (likely <5 Ma) in the Houtman and Zeewyck Sub basins, Western Australia margin northeast of the PAP (Fig. 2a); they are inferred to form by small degrees of partial melting from an enriched (possibly plume) source at depth (involving a garnet bearing source; Dadd et al., 2015). Site 7 displays similar LREE enrichments to basaltic samples from the Kerguelen Archipelago and Western Australia margin basanites (Fig. 7a–e), possibly a result of similar melting conditions and/or depth of melting.

Basalts from Site 6 display enrichment of LILE, HFSE, and LREE comparable to Site 7, but with HREE concentrations similar to those from Site 5 (Fig. 6a). As such, these rocks represent both a compositional and geographical transition between southern MORB-type magmatism (Site 5) and northern OIB-type volcanism (Site 7). Samples from Site 6 are interpreted as a result of mixing of an NMORB and a more enriched source. Site 6 has a geochemical signature similar to Enriched MORB (EMORB), which is commonly associated with, but not exclusively related to plumes (Gale et al., 2013). Negative Ce anomalies and enrichments of La in most of the samples from Site 6 (excluding DR6-9) are characteristic of seawater alteration (Fig. 6a; Verma, 1992). Elevated CaO in these samples is likely a result of the calcite vein network observed in

hand specimen (Table 4). These samples also showed distinctive linear trends in $[Nb/La]_{PM}$ and $[La/Sm]_{PM}$ (Fig. 7b and e), which could be attributed to partial melting or reflect decreases in the extent of melting over time (Sun et al., 1979). Site 6 basalt shows compositional similarity to volcanism from the Central Kerguelen Plateau/Broken Ridge in terms of $[Ce/Y]_N$, $[Nb/La]_N$, $[Th/Nb]_N$, $[Nb/Y]_N$, and $[Zr/Ti]_N$ abundances (Fig. 7a–d), generally accepted to be the most productive phase of the Kerguelen plume in terms of magma output volume and rate (Site 1138–100 Ma; Mahoney et al., 1995; Coffin et al., 2002; Duncan, 2002), around the time of the cessation of spreading in the DHR (~102 Ma). There are also compositional similarities between Site 6 volcanism and the tholeiitic samples from the Naturaliste Plateau in ratios: $[Ce/Y]_N$, $[Zr/Ti]_N$ $[Sm/Yb]_N$, $[Nb/La]_N$, and $[Nb/Y]_N$ (Fig. 7a–e). Although the Naturaliste Plateau tholeiites are not basement samples, instead they make up a volcanic conglomerate overlying the basement, they are attributed to a locally derived early Kerguelen plume source (Ford, 1975; Coleman et al., 1982; Storey et al., 1992; Mahoney et al., 1995).

The Sonne Ridge is a high bathymetric relief linear NNE trending extinct ridge between the Wallaby and Exmouth plateaux offshore Western Australia (Fig. 2a). Volcanic rocks from the more northerly Sonne Ridge show some enrichment of incompatible trace elements, with ratios for $[Nb/Y]_{PM}$, $[Th/Nb]_{PM}$, $[Nb/La]_{PM}$, $[Ce/Y]_{PM}$, $[Zr/Ti]_{PM}$, $[Ti/Y]_{PM}$, and $[Nb/Zr]_{PM}$ comparable to Site 6 on the DHR (Fig. 7a–d). The weakly enriched geochemical signature of these volcanic rocks, coupled with the pronounced bathymetric expression of the Sonne Ridge, provides supporting evidence that a weakness in oceanic crust—either as a pseudofault or an extinct ridge, can act as a conduit for younger melt (Dadd et al., 2015). By analogy, this suggests that the enriched melts from Sites 6 and 7 could be related to later excess volcanism subsequent to ridge cessation, that may have been sourced by pulses of volcanism associated with the Kerguelen plume (e.g., Broken Ridge ~95 Ma or North Kerguelen Plateau ~40 Ma; Coffin et al., 2002; Duncan, 2002).

5. Discussion

5.1. Spreading history and abyssal seafloor morphology

Mesozoic ocean crust in the PAP generated before the CQZ was associated with ~35 mm/yr (half) spreading rates based on magnetic anomalies (Fig. 2a; Williams et al., 2013). Between M0 (~121 Ma) and the onset of spreading in the Wharton Basin, ~1050 km of oceanic crust was produced (including the DHR; Fig. 3a), but any changes in spreading rate are difficult to discern for this period due to the absence of magnetic reversals during the CQZ. Assuming spreading in the PAP remained constant at 35 mm/yr, cessation of spreading would have occurred at 108 Ma (Gibbons et al., 2012). Alternatively, Williams et al. (2013) speculated that a decrease in spreading rate occurred and estimated that final cessation of spreading occurred at 101–103 Ma, to closely precede the initiation of spreading in the Wharton Basin at ~101 ± 1 Ma (Fig. 2a; DSDP Site 256; Davies et al., 1974). Recent $^{40}Ar/^{39}Ar$ dating of plagioclase from gabbroic sample DR5-56 constrains crystallisation to 102.3 ± 2.5 Ma (Whittaker et al., in review). These temporal constraints substantiate a decrease in spreading rate during the CQZ.

We use changes in bathymetric roughness as a proxy for changes in spreading rates due to the apparent symmetry of the region of rough ocean floor about the DHR (see Section 4.1; Fig. 3a). Increased basement roughness is related to slower spreading rates, oblique spreading (>45°), and elevated mantle fertility and/or mantle temperature (Sempéré and Cochran, 1997; Whittaker et al., 2008). Multibeam bathymetric profiles from the PAP (Fig. 3a, c and d) reveal a change from relatively smooth abyssal hill fabric during the Late Mesozoic, to rougher, more irregular ocean crust shortly after the onset of CQZ at 121 Ma. Variation in slope strongly increases towards the DHR, which we attribute to continued slowing in seafloor spreading rates (Fig. 3b). The defined region of increased roughness, spanning ~600 km from east to west, suggests a decrease in spreading rate, consistent with that proposed by Williams et al. (2013). Assuming a constant spreading rate of 35 mm/yr from 121 Ma to the onset of the rougher basement, suggests the slowdown in spreading to ~24 mm/yr half-spreading rate occurred at ~114 Ma. We further suggest a slowdown in spreading rate was likely approaching complete cessation of spreading at ~102 Ma. The concept of a progressive slowdown before full ridge cessation has been previously suggested by numerous studies of extinct ridges around the world (Grevemeyer et al., 1997; Livermore et al., 2000; Downey et al., 2007; Gaina et al., 2007). Such a slowdown is analogous to cessation of spreading at other fossil-spreading centres such as the Aegir Ridge in the Norwegian Sea (Jung and Vogt, 1997), the Osbourn Trough in the West Pacific (Worthington et al., 2006; Downey et al., 2007) and the Galapagos Rise in the East Pacific (Haase et al., 2011b), which all show evidence for a gradual slowdown in spreading, until ridge abandonment. During slow spreading (<55 mm/yr full spreading rate), detachment faulting can exhume lower crust and even mantle rocks to the surface (Cannat, 1993; Dick et al., 2003; Cannat et al., 2006; Escartín et al., 2008; Tucholke et al., 2008; Gerya, 2012). In the PAP, we suggest the 12 million year period of slowing spreading (from 114 Ma to 102 Ma at ≤24 mm/yr) resulted in both increased seafloor roughness and the exhumation of lower crustal gabbros such as those dredged from Site 5 on the DHR. However, a deceleration in spreading rate does not explain how lower crustal rocks were uplifted to the Dirck Hartog Ridge crest (Site 5), ~2 km above surrounding ocean floor (discussed in detail in Sections 5.3 and 5.4).

5.2. Dirck Hartog Ridge volcanism

Our geochemical analyses show there are a range of magmatic processes operating at the DHR: from volcanism geochemically similar to Indian Ocean MORB in the south (Site 5), to EMORB-like at Site 6 and compositionally similar to volcanism on the Central Kerguelen Plateau/Broken Ridge, to highly enriched (OIB-type) small degree melts from greater depth in the north (Site 7).

Although the sample set is small, we suggest that it accurately reflects a trend of increasing alkalinity and incompatible trace element concentrations northward on the DHR. In the south, the geochemical signature of basaltic samples from Site 5 are transitional between DMORB and NMORB (characteristic of mid mid-oceanic ridges >500 km from a hotspot as defined by Gale et al., 2013) and are interpreted to be typical of a mid-oceanic ridge setting (Figs. 6a and 7a).

We suggest two possibilities for the origin of the highly enriched lavas at Sites 6 and 7. One scenario is that the enrichment may be predominantly caused by tectonic drivers and excess volcanism, i.e., decreasing spreading rates, and thickening of the lithosphere during ridge cessation, combined with melting of a heterogeneous mantle and the continuation of volcanism subsequent to ridge cessation (Cannat, 1996; Choe et al., 2007; Haase et al., 2011a, b; Dadd et al., 2015). It is widely recognised that spreading ridges respond to both mantle processes and regional plate motions, which can lead to the extinction or relocation of ridge axes (Haase et al., 2011a). Reunion plume dynamics in the West Indian Ocean are proposed to have considerably influenced local and regional tectonics, from the abandonment of spreading centres, to accelerating, decelerating, and/or changing the direction of continental plates (Cande and Stegman, 2011). In the Indian Ocean, Müller et al. (2000) report that abandonment and relocation of spreading centres are most likely a result of successive ridges propagating towards lithosphere already weakened by plume activity. As spreading rates decline, so the extent of melting is reduced, resulting in preferential melting of "enriched blobs" and elevated LREE/HREE ratio lavas (Haase et al., 2011a, b). In some cases, enriched volcanism can continue after ridge cessation, known as excess volcanism, which forms bathymetric highs along the extinct ridge axis (Haase et al., 2011a, b). Greater depth of melting (Shen and Forsyth, 1995; Choe et al., 2007) due to slower spreading is supported by high $[Sm/Yb]_N$ ratios (i.e., >4 in Site 7

lavas). In this scenario, similarities between the Kerguelen plume lavas and the DHR lavas at Sites 6 and 7 are attributed to similarities in depth and degree of partial melting rather than a common source.

Alternatively, in a second scenario, if similarities between the volcanism on the DHR and that of the Kerguelen plume were a result of a common plume source, then the DHR may have been a zone of lithospheric weakness during and/or after cessation of spreading, which acted as a conduit for plume magmas at a time of substantial Kerguelen plume upwelling. In the East Indian Ocean, the Kerguelen plume continued to produce large volumes (total volume ~2.5×10^7 km^3; Coffin et al., 2002) of magma during the separation of the Australian, Antarctic, and Indian continents and still remains active beneath the Antarctic plate today. The Central Kerguelen Plateau was the site of dominant volcanism just after ridge cessation in the PAP and at ~100 Ma was ~820 km from the DHR. Plate tectonic and mantle models place the Kerguelen plume between 450 and 1300 km from the DHR (Müller et al., 1993; O'Neill et al., 2005; Doubrovine et al., 2012). Plume upwelling has been proposed to influence oceanic lithosphere and mid-ocean ridges within a 1400 km radius (Ribe, 1997), placing the West PAP within the potential region of Kerguelen plume influence.

A difficulty is the apparent absence of plume influence on the rocks formed at Site 5, while basalts further north at Sites 6 and 7 show a possible plume influence. $^{40}Ar/^{39}Ar$ dating constrains the formation of the gabbros at Site 5 to 102.3 ± 2.5 Ma, but no age constraints are yet available for Sites 6 and 7. A possible formation scenario is that the oceanic floor of the PAP and the extinction of the DHR were complete by ~102 Ma during a period of little influence from the Kerguelen Plume, and that a later phase of Kerguelen plume activity formed the basalts at Sites 6 and 7 (e.g., Broken Ridge ~95 Ma or North Kerguelen Plateau ~40 Ma; Coffin et al., 2002; Duncan, 2002).

Supporting evidence for a plume influence on the DHR at some stage of its formation comes from the morphology of the West PAP. The West PAP is distinctly shallower and has more varied bathymetry than the East PAP. In particular, the ENE–WSW trending elongate ridge in the centre of the West PAP (see Fig. 2d and description in Section 4.1) has striking similarities with the Rodrigues Ridge in the Central Indian Ocean (Fig. 1). The Rodrigues Ridge reflects one type of plume–ridge interaction, where material from the plume connects with the ridge by eroding a channel into the overlying lithosphere, or by tensional fissures, to allow melt to ascend causing relief and distinctive linear bathymetric flow lines (Sleep, 2002; Dyment et al., 2007; Sleep, 2008). In addition, like the volcanism on the DHR, basaltic samples recovered from the active Central Indian Ridge to the east of the Rodrigues Ridge (between 18°S and 25°S) show a range of composition from NMORB to incompatible element-enriched basalts believed to be a result of plume–asthenosphere mixing (Murton et al., 2005).

The unusual morphology and the uneven irregular bathymetry in the West PAP (detailed in Section 5.1; Sleep, 1996) supports the Kerguelen plume as a source for the enriched volcanism on the DHR (Sites 6 and 7) through magmatic underplating and lateral flow of plume material towards the DHR. During or subsequent to spreading in the PAP, we suggest that the underplating of Kerguelen plume material could explain the increased seafloor relief in the West PAP.

Pb, Nd, and Sr isotopic ratios in early volcanism from the South Kerguelen Plateau are interpreted to reflect assimilation of continental crust (Frey et al., 2000; Ingle et al., 2002). There is also evidence for continental volcanism prior to the breakup of East Gondwana (Comei Large Igneous Province—132 Ma and the Early Cretaceous basaltic rocks from the Cona area in Tibet; Zhu et al., 2008; Zhu et al., 2009); however, the role of the Kerguelen plume in the breakup of East Gondwana remains unresolved. Nevertheless, the combined interaction from three end member sources: (1) Kerguelen plume material, (2) Gondwanan continental lithosphere, and (3) depleted mantle, played a major role in creating highly varied heterogeneous volcanism in the Indian Ocean (Ingle et al., 2002; Mahoney et al., 2002; Neal et al., 2002). Further isotopic analyses and Ar–Ar dating of basaltic samples could better constrain the relationship between the Kerguelen plume and the DHR volcanism.

5.3. Tectonic plate reorganisation and the formation of Dirck Hartog Ridge

It was not exclusively plume-derived volcanism that resulted in the unusual present day morphology of the Indian Ocean floor (Ingle et al., 2002). The cessation of proto-Pacific ocean floor subduction beneath Eastern Gondwana likely caused the observed global scale reorganisation of tectonic plates 105–100 Ma (Matthews et al., 2012) and may also have led to the final stages of spreading in the PAP. This significant tectonic reorganisation of the Indian plate resulted in the distinctive bending fracture zones and unique seafloor fabric in the Wharton Basin (Fig. 2a and d). Uncertainties remain as to the true extent of influence the Kerguelen plume and major tectonic plate reorganisation had on rifting, volcanism, and morphology in the PAP.

The morphology of the southern DHR is highly irregular and distinctly asymmetric, with pronounced relief and positive gravity anomalies along the ridge crest (Section 4.1; Fig. 8a). Extinct spreading centres globally, of varying age consistently show subtle, if any, surface expression and can be very difficult to identify without magnetic anomalies. On the western side of the Indian Ocean in the Western Somali Basin (Fig. 1), a conjugate set of Mesozoic magnetic anomalies are used to identify an extinct spreading centre of age M9 (128 Ma; Coffin and Rabinowitz, 1987). Considering both the Western Somali Extinct Ridge and the DHR formed around the same time, similar rates of ocean floor subsidence are expected. Unlike the DHR, the Western Somali Extinct Ridge has almost no gravity variation across the ridge axis, making it extremely difficult to identify (Fig. 8b; Coffin et al., 1986; Small, 1989). In the western Pacific Ocean, the Osbourn Trough extinct spreading centre, like the DHR, was also active predominantly during the CQZ (Downey et al., 2007). The lack of polarity reversals during the formation of the Osbourn Trough has meant the identification of this fossil-spreading centre was largely based on morphological characteristics (gravity and bathymetry) and the recovery of Pacific MORB-type lavas in the paleo rift valley (Worthington et al., 2006). Similar to the PAP, the abyssal fabric surrounding the Osbourn Trough shows increased roughness towards the paleo ridge axis, interpreted as a slowdown in spreading rate before cessation (Worthington et al., 2006; Downey et al., 2007). However, the morphology of the Osbourn Trough is much less pronounced than the southern DHR (Fig. 8c) and is distinguished by a bathymetric and gravity depression rather than a high relief ridge structure, with variable lava composition like the DHR.

The Phoenix Ridge in the Drake Passage (extinct 3.3 Ma) is an example of an extinct spreading ridge with unusual high relief ridge and positive gravity anomalies along the ridge axis, comparable to the DHR and atypical of extinct ridges in other regions (Fig. 8d; Livermore et al., 2000; Haase et al., 2011a). It is well documented that spreading on the Phoenix Ridge became unviable as a response to regional changes in tectonic regime. This resulted in enriched excess volcanism derived from low degrees of melting to continue 2 Myr after ridge cessation, forming the unusual high relief ridge axis (Livermore et al., 2000; Choe et al., 2007). It is possible that the high relief DHR and enriched alkali basalts recovered from Sites 6 and 7 may also be a manifestation of excess volcanism during and subsequent to ridge cessation. However, the DHR shows considerably higher relief than the Phoenix Ridge. This is striking, considering the effects of ocean floor subsidence on the relatively young extinct Phoenix Ridge are negligible compared to the 100 million year old DHR. Furthermore, excess volcanism on the DHR cannot explain the recovery of gabbroic samples at Site 5. Finally, the DHR also differs substantially from active mid-oceanic ridges currently forming at slow spreading rates, such as the Central Indian Ridge (segment from 20°S to 25°S, spreading at ~48.7 mm/yr full spreading; Small, 1989; Fig. 1). Compared to the DHR, the Central Indian Ridge shows much smaller and more regular variations in gravity and bathymetry across the axis (Fig. 8e).

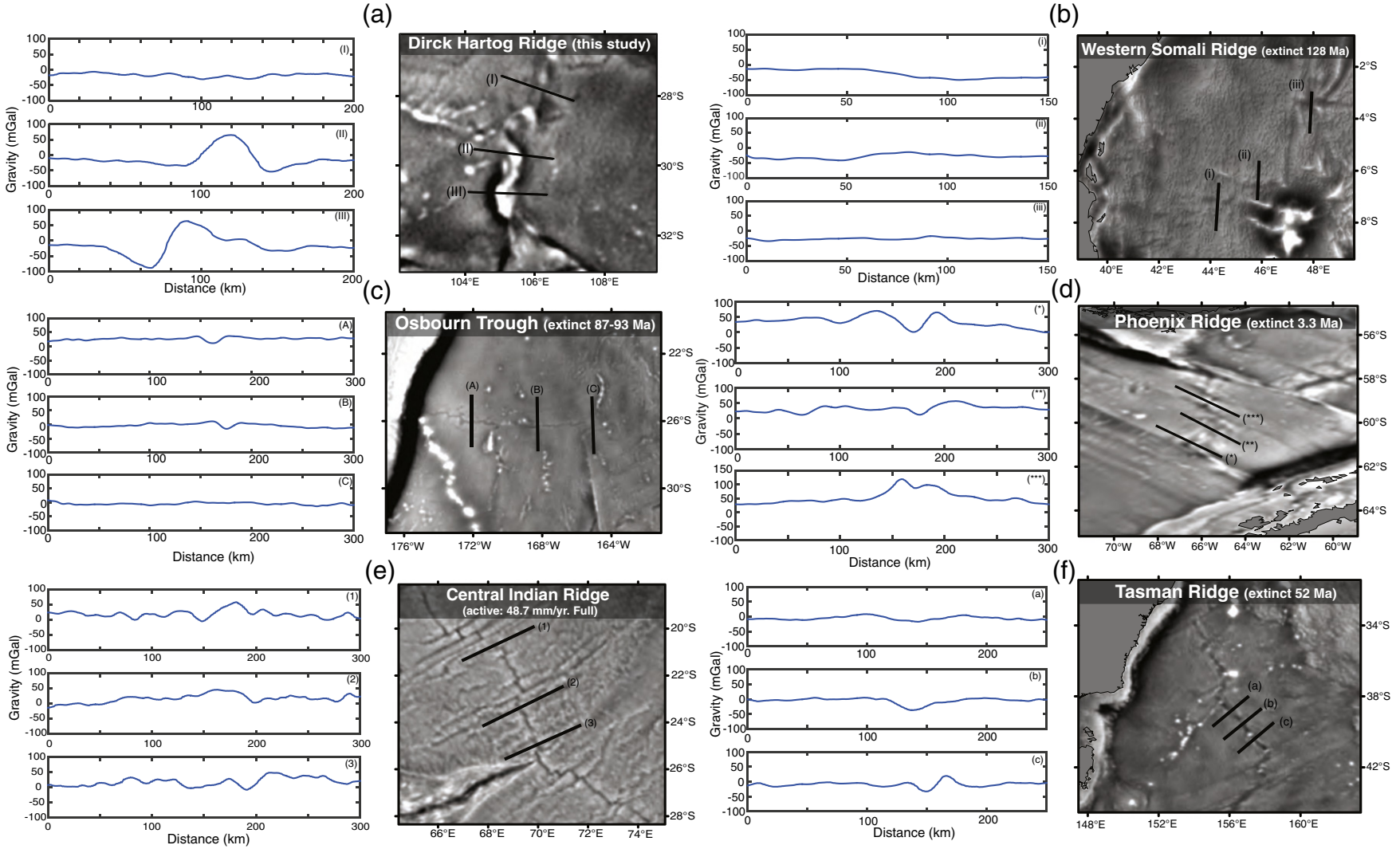

Fig. 8. Gravity map (Sandwell and Smith, 2009) and transverse profiles of extinct ridges from around the world to show differences in morphology compared to the Dirck Hartog Ridge. (a) The Dirck Hartog Ridge; extinct ~102 Ma. (b) The West Somali Extinct Ridge; extinct 128 Ma. (c) The Osbourn Trough; extinct by 87–93 Ma. (d) The Phoenix Ridge; extinct 3.3 Ma. (e) The Central Indian Ridge; active, 48.7 mm/yr full spreading rate. (f) The Tasman Extinct Ridge; extinct 52 Ma.

The morphology of the DHR is not typical of other regional examples of extinct spreading centres, which frequently display much lower relief and more muted bathymetric and gravity expression, e.g., the Tasman Extinct Ridge in the Tasman Sea (Fig. 8f; extinct 52 Ma; Gaina et al., 1998) and the Enderby Basin Extinct Ridge (extinct ~120 Ma; Gaina et al., 2007). The highly unusual morphology of the DHR together with gabbros dredged from the southern ridge crest ~2 km above the surround seafloor (Site 5), suggests a tectonic mechanism is required to elevate these unroofed lower crustal rocks to the apex of the ~2 km high southern DHR axis.

The southern tip of the DHR meets the Naturaliste Fracture Zone at 31°S, 105°E (Fig. 2a). During seafloor spreading in the PAP, if the Naturaliste Fracture Zone acted as a transform offset fault, the elevated southern DHR would have formed an inner ridge–transform intersection. Ridge–transform intersections (especially those associated with slower spreading) are locations where oceanic core complexes can form, causing high relief and lower crust exhumation (Karson and Dick, 1983; Dick, 1989; Pockalny et al., 1997; Buck et al., 2005). It is therefore plausible that DHR gabbros were exhumed and elevated via this mechanism.

Alternatively, the unique morphology of the DHR and lower crust dredged from Site 5 could have been a result of a reactivation of the extinct oceanic plate boundary following the cessation of spreading. While the timing of this reactivation is uncertain, it would have occurred after 102 Ma to account for the crystallisation of the plagioclase grains in gabbro from Site 5. Also, oceanic lithosphere strengthens rapidly after it forms (Small, 1995), suggesting that the most likely time for a reactivation event is within 5 Myr of its formation—not long after cessation of spreading in the PAP at ~102 Ma.

5.4. The Perth Abyssal Plain reconstructed: reconciling tectonic drivers and the influence of the Kerguelen plume

Tectonic processes alone can account for some, but not all of the observations in the PAP. The region of roughness spanning ~600 km from east to west (see Section 4.1; Fig. 3a) can be accounted for by a reduced rate of spreading in the PAP's history. A deceleration of spreading rates in the history of the PAP is substantiated by late Albian sediment ages from DSDP Site 256 in the Wharton Basin (Fig. 2a; Davies et al., 1974), and $^{40}Ar/^{39}Ar$ dating of gabbro from the southern DHR (Site 5) to

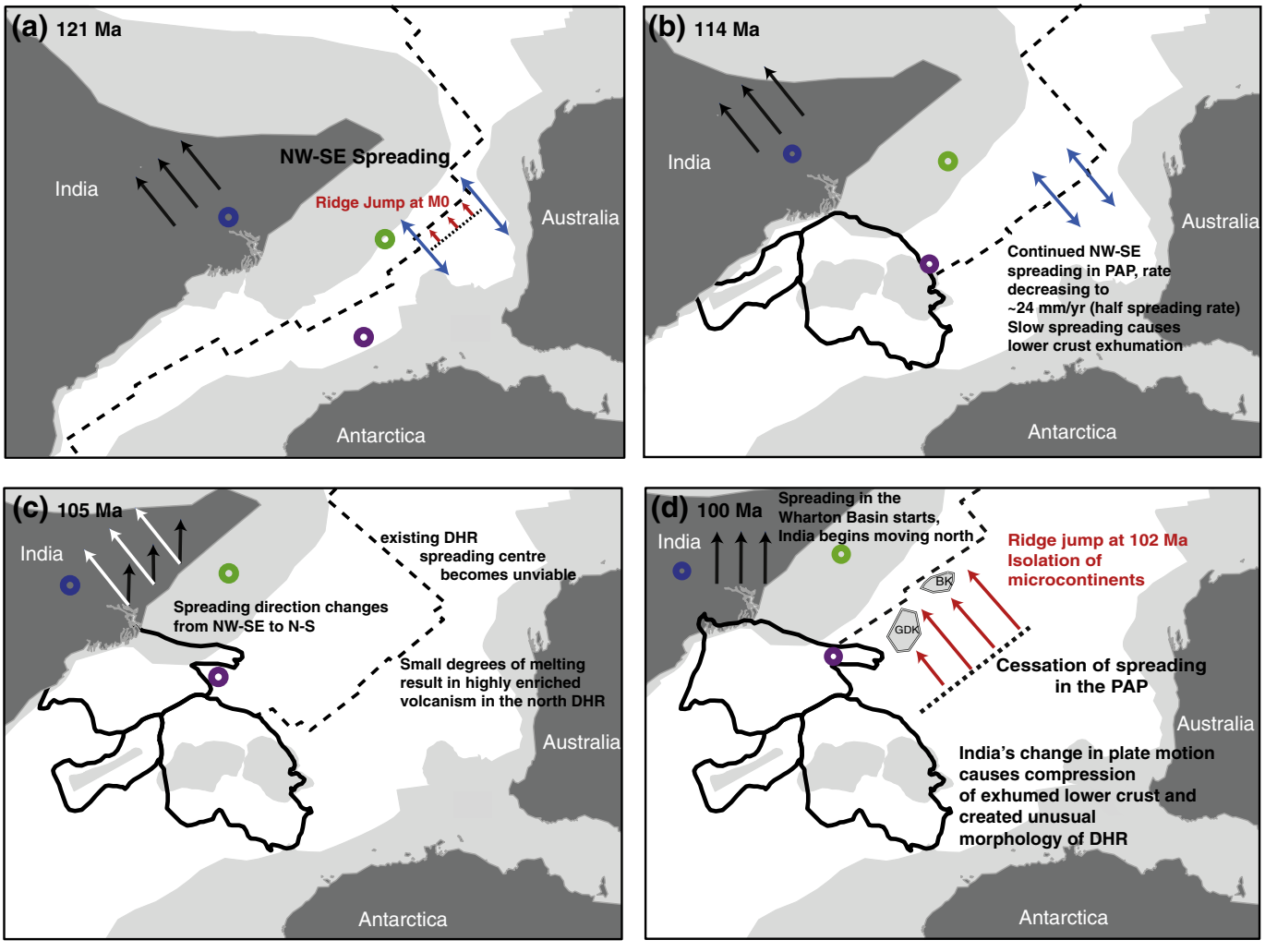

Fig. 9. Tectonic reconstruction of the Perth Abyssal Plain and the formation of the Dirck Hartog Ridge using GPlates reconstruction software (Gibbons et al., 2013). Coloured circles are modelled plume locations: (Müller et al., 1993; purple, O'Neill et al., 2005; blue, Doubrovine et al., 2012; green). Black arrows indicate relative direction of plate motion, red arrows represent ridge jumps, and blue double headed arrows represent plate divergence. (a) Increased seafloor roughness is interpreted as a decrease from intermediate, 35 mm/yr, to (b) slow half spreading rates, 24 mm/yr beginning at ~114 Ma until ridge cessation at ~102 Ma resulting in increased seafloor roughness and the exhumation of lower crustal gabbros. (c) Changes in India's plate motion from NW–SE to N–S in response to a major tectonic reorganisation initiated at ~105 Ma. During or subsequent to ridge cessation (~102 Ma), highly enriched excess volcanism manifests on the Dirck Hartog Ridge. White arrows show initial direction of plate motion for comparison. (d) Subsequent to cessation of spreading in the Perth Abyssal Plain (~102 Ma), India's change in plate motion isolated microcontinental blocks (Batavia and Gulden Draak knolls) and caused compression of the Dirck Hartog Ridge, uplifting exhumed lower crust and resulting in the high relief and unusual morphology of this now extinct mid-ocean ridge.

102.3 ± 1.5 Ma (see Section 2.2; Whittaker et al., in review). Reduced rates of spreading can also result in the exhumation of lower crust (Site 5; Escartín et al., 2008) and enriched volcanism (Haase et al., 2011a; Sites 6 and 7) as the total volume of melt able to reach the surface is reduced.

The depth and the morphological asymmetry between the East and the West PAP are difficult to reconcile exclusively with plate tectonic processes and are more likely to be associated with an episodic plume influence. Also, it is unlikely that successive ridge jumps would occur in the evolution of the PAP without some degree of plume influence to weaken the overlying lithosphere (Müller et al., 2001). The interaction between tectonic plates and plume influence in the PAP can be compared to the formation of the Enderby Basin, offshore East Antarctica (Fig. 1). The spreading centre in the Enderby Basin was producing crust at a rate of 28–65 mm/year (half spreading rate) and became extinct by ~115 Ma (Gibbons et al., 2013). During the Early Cretaceous separation of East Gondwana, the Enderby Basin and the PAP were joined to form a continuous spreading system between the Asia-bound Indian continent and Australia–Antarctica. Analogous to the PAP, the Enderby Basin was influenced by both the Kerguelen plume and continental rifting, experiencing ridge jumps that isolated a continental fragment in the southern Indian Ocean—the Elan Bank (Ramana et al., 2001; Gaina et al., 2007; Gibbons et al., 2013). Although these basins formed at a similar time and in comparable conditions, the extinct ridge that formed the Enderby Basin is almost indistinguishable from surrounding ocean floor in both bathymetry and gravity, very unlike the DHR. So what geologic processes could be responsible for creating such a unique extinct ridge in the PAP, which did not occur the Enderby Basin?

Here, we propose a tectonic history of the PAP that explains all the observed geophysical, geochemical, and geochronological data available across the PAP with particular focus on detailing the formation of the DHR. Subsequent to the westward ridge jump at M0 (121 Ma), spreading in the PAP continued at 35 mm/yr until 114 Ma (Fig. 9a). From 114 Ma, a decrease in the rate of seafloor spreading resulted in increased seafloor roughness and the formation of oceanic core complexes in the vicinity of the DHR by exhumation of the lower crust along detachment faults (Section 5.1; Fig. 9b). Highly enriched volcanic rock manifested at the surface of the DHR either as excess volcanism (a result of slowing spreading rates and melting of a heterogeneous mantle source) or derived from magmatic pulses of Kerguelen plume material subsequent to the cessation of spreading.

From 95 to 105 Ma, a change in the relative motion of the Indian plate occurred, possibly as part of a major global tectonic plate reorganisation event (Fig. 9c; Matthews et al., 2012). Consequently, relative plate configuration and movement reorganised the direction of spreading between India and the Australian–Antarctic plates from dominantly NW–SE to N–S spreading. This radical change in plate motion resulted in the bending of fracture zones in the Wallaby-Zenith Fracture Zone (detailed by Matthews et al., 2012; Müller et al., 2000) and likely invoked major stresses on the DHR. We suggest the Indian–Australian plate reorganisation event may have caused compression and deformation of the recently abandoned DHR. The anticlockwise rotation of the Indian Plate (detailed in Matthews et al., 2012) would have lead to concentrated compressive forces in the southern DHR. The rapid change in tectonic regime from extension to compression resulted in the inversion of normal low-angle detachment faults causing uplift of exhumed gabbros to form the high relief and axial asymmetry of the DHR (Fig. 9d) and could explain the observed 15°–18° offset between the Mesozoic magnetic anomalies and abyssal hill fabric in the West PAP compared to the East PAP (Section 4.1).

6. Conclusions

Geological data and swath bathymetry supports recent interpretations based on magnetic anomalies that the DHR is an extinct spreading ridge rather than a pseudofault. This study presents the first analyses of mafic volcanic and intrusive rocks collected from the previously unexplored DHR. Geochemical data reveal significant compositional variations that are associated with varied melting conditions and source. The geochemical results of the current study cannot definitively link the DHR volcanism to the voluminous upwelling of the Kerguelen plume, although plume activity is considered to contribute to mantle heterogeneity and promote ridge jumps. The depth and morphological asymmetries between the East and West PAP could be evidence for plume–ridge interaction in the West PAP. If the plume is responsible for the enriched signature of northern DHR basalts, the extent of influence of the Kerguelen plume would have exceeded 1000 km. Additional sampling and/or isotopic analyses of current samples would assist by further constraining the source of volcanism on the DHR.

We suggest the Kerguelen plume had an episodic influence throughout the history of the PAP, during a time of major tectonic plate motion and supercontinental dispersal. Geologic and geophysical data presented in this study demonstrates the significance of regional tectonic plate motion on the deformation of young ocean crust, and provides insight into the formation of unique morphology of a Cretaceous mid-ocean ridge.

Acknowledgements

The figures in this paper were created using GPlates, ArcGIS, GMT, and Matlab.

We are grateful to Dr. Roland Maas, Alan Greig (School of Earth Sciences, University of Melbourne), Alexander Cuison, and Katie and Peter McGoldrick (School of Earth Sciences, University of Tasmania) for their knowledge, assistance, and expertise in geochemical preparation and analyses. We thank Fred Frey and an anonymous reviewer for their constructive comments that greatly improved this paper. This work was only possible with the support of the crew and scientific party aboard voyage SS2011_V06 of Australia's Marine National Facility, *R/V Southern Surveyor*. We also thank Statoil for providing additional financial support to for this voyage. Finances for geochemical analyses undertaken in 2015 were supported by a University of New England 'seed grant' (A14/1876; 2015). J.W. was supported by Australian Research Council grant DE140100376. This research was supported under the Australian Research Council's Special Research Initiative for Antarctic Gateway Partnership (Project ID SR140300001).

Appendix A. Supplementary data

Supplementary data to this article can be found online at http://dx.doi.org/10.1016/j.gr.2016.03.009.

References

Beccaluva, L., Ohnenstetter, D., Ohnenstetter, M., Venturelli, G., 1977. The trace element geochemistry of Corsican ophiolites. Contributions to Mineralogy and Petrology 64 (1), 11–31.

Buck, W.R., Lavier, L.L., Poliakov, A.N.B., 2005. Modes of faulting at mid-ocean ridges. Nature 434 (7034), 719–723. http://dx.doi.org/10.1038/nature03358.

Cande, S.C., Stegman, D.R., 2011. Indian and African plate motions driven by the push force of the Reunion plume head. Nature 475 (7354), 47–52. http://dx.doi.org/10.1038/nature10174.

Cannat, M., 1993. Emplacement of mantle rocks in the seafloor at mid-ocean ridges. Journal of Geophysical Research—Solid Earth 98 (B3), 4163–4172. http://dx.doi.org/10.1029/92JB02221.

Cannat, M., 1996. How thick is the magmatic crust at slow spreading oceanic ridges? Journal of Geophysical Research—Solid Earth 101 (B2), 2847–2857. http://dx.doi.org/10.1029/95JB03116.

Cannat, M., Sauter, D., Mendel, V., Ruellan, E., Okino, K., Escartin, J., ... Baala, M., 2006. Modes of seafloor generation at a melt-poor ultraslow-spreading ridge. Geology 34 (7), 605–608. http://dx.doi.org/10.1130/G22486.1.

Carbotte, S.M., Macdonald, K.C., 1994. Comparison of seafloor tectonic fabric at intermediate, fast, and super fast spreading ridges: Influence of spreading rate, plate motions, and ridge segmentation on fault patterns. Journal of Geophysical Research: Solid Earth (1978–2012) 99 (B7), 13609–13631.

Choe, W.H., Lee, J.I., Lee, M.J., Hur, S.D., Jin, Y.K., 2007. Origin of E-MORB in a fossil spreading center: the Antarctic–Phoenix Ridge, Drake Passage, Antarctica. Geosciences Journal 11 (3), 185–199. http://dx.doi.org/10.1007/BF02913932.
Coffin, M.F., Rabinowitz, P.D., 1987. Reconstruction of Madagascar and Africa: Evidence from the Davie Fracture Zone and Western Somali Basin. Journal of Geophysical Research—Solid Earth 92 (B9), 9385–9406. http://dx.doi.org/10.1029/JB092iB09p09385.
Coffin, M.F., Rabinowitz, P.D., Houtz, R.E., 1986. Crustal structure in the Western Somali Basin. Geophysical Journal International 86 (2), 331–369. http://dx.doi.org/10.1111/j.1365-246X.1986.tb03832.x.
Coffin, M.F., Pringle, M.S., Duncan, R.A., Gladczenko, T.P., Storey, M., Müller, R.D., Gahagan, L.A., 2002. Kerguelen Hotspot Magma Output since 130 Ma. Journal of Petrology 43 (7), 1121–1137. http://dx.doi.org/10.1093/petrology/43.7.1121.
Coleman, P.J., Michael, P.J., Mutter, J.C., 1982. The origin of the Naturaliste Plateau, SE Indian Ocean: Implications from dredged basalts. Journal of the Geological Society of Australia 29 (3–4), 457–468. http://dx.doi.org/10.1080/00167618208729228.
Crostella, A., Backhouse, J., 2000. Geology and Petroleum Exploration of the Central and Southern Perth Basin, Western Australia. Geological Survey of Western Australia.
Dadd, K.A., Kellerson, L., Borissova, I., Nelson, G., 2015. Multiple sources for volcanic rocks dredged from the Western Australian rifted margin. Marine Geology 368, 42–57. http://dx.doi.org/10.1016/j.margeo.2015.07.001.
Davies, T.A., Luyendyk, B.P., 1974. Initial Reports of the Deep Sea Drilling Project, 26 (Initial DSDP Report No. 26). U.S. Government Printing Office (Retrieved from http://deepseadrilling.org/26/dsdp_toc.htm).
Davies, T.A., Luyendyk, B.P., et al., 1974. Initial Reports of the Deep Sea Drilling Project, 26 vol. 26. U.S. Government Printing Office (Retrieved from http://deepseadrilling.org/26/dsdp_toc.htm).
Deep Sea Drilling Project, 1989. Archive of Core and Site/Hole Data and Photographs from the Deep Sea Drilling Project (DSDP). http://dx.doi.org/10.7289/V54M92G2 (Retrieved from https://www.ngdc.noaa.gov/mgg/geology/dsdp/dsdpcdv2.htm).
Dick, H.J.B., 1989. Abyssal Peridotites, very Slow Spreading Ridges and Ocean Ridge Magmatism. Magmatism in the Ocean Basins 42 pp. 71–105.
Dick, H.J., Robinson, P.T., Meyer, P.S., 1993. The plutonic foundation of a slow-spreading ridge. Synthesis of Results from Scientific Drilling in the Indian Ocean, pp. 1–39.
Dick, H.J.B., Lin, J., Schouten, H., 2003. An ultraslow-spreading class of ocean ridge. Nature 426 (6965), 405–412. http://dx.doi.org/10.1038/nature02128.
Divins, D.L., 2003. Total sediment thickness of the world's oceans & marginal seas. NOAA National Geophysical Data Center (Retrieved from https://www.ngdc.noaa.gov/mgg/sedthick/sedthick.html).
Doubrovine, P.V., Steinberger, B., Torsvik, T.H., 2012. Absolute plate motions in a reference frame defined by moving hot spots in the Pacific, Atlantic, and Indian oceans. Journal of Geophysical Research—Solid Earth 117 (B9), B09101. http://dx.doi.org/10.1029/2011JB009072.
Downey, N.J., Stock, J.M., Clayton, R.W., Cande, S.C., 2007. History of the Cretaceous Osbourn spreading center. Journal of Geophysical Research—Solid Earth 112 (B4), B04102. http://dx.doi.org/10.1029/2006JB004550.
Duncan, R.A., 2002. A Time Frame for Construction of the Kerguelen Plateau and Broken Ridge. Journal of Petrology 43 (7), 1109–1119. http://dx.doi.org/10.1093/petrology/43.7.1109.
Dyment, J., Lin, J., Baker, E.T., 2007. Ridge–Hotspot Interactions; What Mid-Ocean Ridges Tell us about Deep Earth Processes. Special Issue on InterRidge 20(1) pp. 102–115.
Escartín, J., Smith, D.K., Cann, J., Schouten, H., Langmuir, C.H., Escrig, S., 2008. Central role of detachment faults in accretion of slow-spreading oceanic lithosphere. Nature 455 (7214), 790–794. http://dx.doi.org/10.1038/nature07333.
Ford, A.B., 1975. Volcanic rocks of Naturaliste Plateau, Eastern Indian Ocean, Site 264, DSDP Leg 28. Initial Reports of the Deep Sea Drilling Project vol. 28, pp. 821–833.
Frey, F.A., McNaughton, N.J., Nelson, D.R., deLaeter, J.R., Duncan, R.A., 1996. Petrogenesis of the Bunbury Basalt, Western Australia: interaction between the Kerguelen plume and Gondwana lithosphere? Earth and Planetary Science Letters 144 (1–2), 163–183. http://dx.doi.org/10.1016/0012-821X(96)00150-1.
Frey, F.A., Coffin, M.F., Wallace, P.J., Weis, D., Zhao, X., Wise Jr., S.W., ... Antretter, M., 2000. Origin and evolution of a submarine large igneous province: the Kerguelen Plateau and Broken Ridge, southern Indian Ocean. Earth and Planetary Science Letters 176 (1), 73–89. http://dx.doi.org/10.1016/S0012-821X(99)00315-5.
Frey, F.A., Nicolaysen, K., Kubit, B.K., Weis, D., Giret, A., 2002. Flood Basalt from Mont Tourmente in the central Kerguelen Archipelago: the Change from Transitional to Alkalic Basalt at ~25 Ma. Journal of Petrology 43 (7), 1367–1387. http://dx.doi.org/10.1093/petrology/43.7.1367.
Gaina, C., Müller, R.D., Royer, J.-Y., Stock, J., Hardebeck, J., Symonds, P., 1998. The tectonic history of the Tasman Sea: A puzzle with 13 pieces. Journal of Geophysical Research—Solid Earth 103 (B6), 12413–12433. http://dx.doi.org/10.1029/98JB00386.
Gaina, C., Müller, R.D., Brown, B., Ishihara, T., Ivanov, S., 2007. Breakup and early seafloor spreading between India and Antarctica. Geophysical Journal International 170 (1), 151–169. http://dx.doi.org/10.1111/j.1365-246X.2007.03450.x.
Gale, A., Dalton, C.A., Langmuir, C.H., Su, Y., Schilling, J.-G., 2013. The mean composition of ocean ridge basalts. Geochemistry, Geophysics, Geosystems 14 (3), 489–518. http://dx.doi.org/10.1029/2012GC004334.
Gardner, R.L., Daczko, N.R., Halpin, J.A., Whittaker, J.M., 2015. Discovery of a microcontinent (Gulden Draak Knoll) offshore Western Australia: Implications for East Gondwana reconstructions. Gondwana Research 28 (3), 1019–1031. http://dx.doi.org/10.1016/j.gr.2014.08.013.
Gerya, T., 2012. Origin and models of oceanic transform faults. Tectonophysics *522–523*, 34–54. http://dx.doi.org/10.1016/j.tecto.2011.07.006.
Gibbons, A.D., Barckhausen, U., van den Bogaard, P., Hoernle, K., Werner, R., Whittaker, J.M., Müller, R.D., 2012. Constraining the Jurassic extent of Greater India: Tectonic evolution of the West Australian margin. Geochemistry, Geophysics, Geosystems *13* (5), Q05W13. http://dx.doi.org/10.1029/2011GC003919.
Gibbons, A.D., Whittaker, J.M., Müller, R.D., 2013. The breakup of East Gondwana: Assimilating constraints from Cretaceous ocean basins around India into a best-fit tectonic model. Journal of Geophysical Research—Solid Earth 118 (3), 808–822. http://dx.doi.org/10.1002/jgrb.50079.
Goff, J.A., Ma, Y., Shah, A., Cochran, J.R., Sempéré, J.-C., 1997. Stochastic analysis of seafloor morphology on the flank of the Southeast Indian Ridge: The influence of ridge morphology on the formation of abyssal hills. Journal of Geophysical Research: Solid Earth (1978–2012) 102 (B7), 15521–15534.
Goff, J.A., Smith, W.H., Marks, K.M., 2004. The contributions of abyssal hill morphology and noise to altimetric gravity fabric. Oceanography Washington DC Oceanography Society 17 (1), 24–37.
Grevemeyer, I., Weigel, W., Dehghani, G.A., Whitmarsh, R.B., Avedik, F., 1997. The Aegir Rift: Crustal Structure of an Extinct Spreading Axis. Marine Geophysical Researches 19 (1), 1–23. http://dx.doi.org/10.1023/A:1004288815129.
Haase, K.M., Beier, C., Fretzdorff, S., Leat, P.T., Livermore, R.A., Barry, T.L., ... Hauff, F., 2011a. Magmatic evolution of a dying spreading axis: Evidence for the interaction of tectonics and mantle heterogeneity from the fossil Phoenix Ridge, Drake Passage. Chemical Geology 280 (1–2), 115–125. http://dx.doi.org/10.1016/j.chemgeo.2010.11.002.
Haase, K.M., Regelous, M., Duncan, R.A., Brandl, P.A., Stroncik, N., Grevemeyer, I., 2011b. Insights into mantle composition and mantle melting beneath mid-ocean ridges from postspreading volcanism on the fossil Galapagos Rise. Geochemistry, Geophysics, Geosystems *12* (5), Q0AC11. http://dx.doi.org/10.1029/2010GC003482.
Hart, S.R., Blusztajn, J., Dick, H.J., Meyer, P.S., Muehlenbachs, K., 1999. The fingerprint of seawater circulation in a 500-meter section of ocean crust gabbros. Geochimica et Cosmochimica Acta 63 (23), 4059–4080.
Ingle, S., Weis, D., Scoates, J.S., Frey, F.A., 2002. Relationship between the early Kerguelen plume and continental flood basalts of the paleo-Eastern Gondwanan margins. Earth and Planetary Science Letters 197 (1–2), 35–50. http://dx.doi.org/10.1016/S0012-821X(02)00473-9.
Jones, A.T., Kelman, A.P., Kennard, J., Le Poidevin, S., Mantle, D., Mory, A.J., 2012. Offshore PerthBasin Biozonation and Stratigraphy 2011. Geoscience Australia.
Jung, W.-Y., Vogt, P.R., 1997. A gravity and magnetic anomaly study of the extinct Aegir Ridge, Norwegian Sea. Journal of Geophysical Research—Solid Earth 102 (B3), 5065–5089. http://dx.doi.org/10.1029/96JB03915.
Karson, J.A., 1998. Internal structure of oceanic lithosphere: a perspective from tectonic windows. Geophysical Monograph-American Geophysical Union 106, 177–218.
Karson, J.A., Dick, H.J.B., 1983. Tectonics of ridge–transform intersections at the Kane Fracture Zone. Marine Geophysical Researches 6 (1), 51–98.
Kobler, M. E. (2012). Petrographic, Geochemical and Geochronological Characterisation of Batavia Knoll Dredge Samples, Perth Abyssal Plain: Implications for Linkage with Gondwana. Honours Thesis, Macquarie University, 110 pp, unpublished.
Krishna, K.S., Michael, L., Bhattacharyya, R., Majumdar, T.J., 2009. Geoid and gravity anomaly data of conjugate regions of Bay of Bengal and Enderby Basin: New constraints on breakup and early spreading history between India and Antarctica. Journal of Geophysical Research—Solid Earth 114 (B3), B03102. http://dx.doi.org/10.1029/2008JB005808.
Langmuir, C.H., Klein, E.M., Plank, T., 1992. Petrological Systematics of Mid-Ocean Ridge Basalts: Constraints on Melt Generation Beneath Ocean Ridges. In: Morgan, J.P., Blackman, D.K., Sinton, J.M. (Eds.), Mantle Flow and Melt Generation at Mid-Ocean Ridges. American Geophysical Union, pp. 183–280 (Retrieved from http://onlinelibrary.wiley.com/doi/10.1029/GM071p0183/summary).
Livermore, R., Balanyá, J.C., Maldonado, A., Martínez, J.M., Rodríguez-Fernández, J., Galdeano, C.S.d., ... Viseras, C., 2000. Autopsy on a dead spreading center: the Phoenix Ridge, Drake Passage, Antarctica. Geology 28 (7), 607–610. http://dx.doi.org/10.1130/0091-7613(2000)28<607:AOADSC>2.0.CO;2.
Mahoney, J.J., Jones, W.B., Frey, F.A., Salters, V.J.M., Pyle, D.G., Davies, H.L., 1995. Geochemical characteristics of lavas from Broken Ridge, the Naturaliste Plateau and southernmost Kerguelen Plateau: Cretaceous plateau volcanism in the southeast Indian Ocean. Chemical Geology 120 (3–4), 315–345. http://dx.doi.org/10.1016/0009-2541(94)00144-W.
Mahoney, J.J., Graham, D.W., Christie, D.M., Johnson, K.T.M., Hall, L.S., Vonderhaar, D.L., 2002. Between a Hotspot and a Cold Spot: Isotopic Variation in the Southeast Indian Ridge asthenosphere, 86°E–118°E. Journal of Petrology 43 (7), 1155–1176. http://dx.doi.org/10.1093/petrology/43.7.1155.
Malinverno, A., 1991. Inverse square-root dependence of mid-ocean-ridge flank roughness on spreading rate. Nature 352 (6330), 58–60. http://dx.doi.org/10.1038/352058a0.
Matthews, K.J., Seton, M., Müller, R.D., 2012. A global-scale plate reorganization event at 105 − 100 Ma. Earth and Planetary Science Letters 355–356, 283–298. http://dx.doi.org/10.1016/j.epsl.2012.08.023.
Mihut, D., 1997. Breakup and mesozoic seafloor spreading between the Australian and Indian plates. Retrieved from http://ses.library.usyd.edu.au:80/handle/2123/8940.
Mihut, D., Müller, R.D., 1998. Volcanic margin formation and Mesozoic rift propagators in the Cuvier Abyssal Plain off Western Australia. Journal of Geophysical Research—Solid Earth 103 (B11), 27135–27149. http://dx.doi.org/10.1029/97JB02672.
Müller, R.D., Royer, J.-Y., Lawver, L.A., 1993. Revised plate motions relative to the hotspots from combined Atlantic and Indian Ocean hotspot tracks. Geology 21 (3), 275–278. http://dx.doi.org/10.1130/0091-7613(1993)021<0275:RPMRTT>2.3.CO;2.
Müller, R.D., Roest, W.R., Royer, J.-Y., 1998. Asymmetric sea-floor spreading caused by ridge–plume interactions. Nature 396 (6710), 455–459. http://dx.doi.org/10.1038/24850.
Müller, R.D., Gaina, C., Tikku, A., Mihut, D., Cande, S.C., Stock, J.M., 2000. Mesozoic/Cenozoic tectonic events around Australia. In: Richards, r.A., Gordon, R.G., Hilst, R.D.V.D. (Eds.), The History and Dynamics of Global Plate Motions. American Geophysical Union, pp. 161–188 (Retrieved from http://onlinelibrary.wiley.com/doi/10.1029/GM121p0161/summary).

Müller, R.D., Gaina, C., Roest, W.R., Hansen, D.L., 2001. A recipe for microcontinent formation. Geology 29 (3), 203–206. http://dx.doi.org/10.1130/0091-7613(2001)029<0203:ARFMF>2.0.CO;2.
Murton, B.J., Tindle, A.G., Milton, J.A., Sauter, D., 2005. Heterogeneity in southern central Indian ridge MORB: implications for ridge–hot spot interaction. Geochemistry, Geophysics, Geosystems 6 (3), Q03E20. http://dx.doi.org/10.1029/2004GC000798.
National Oceanic and Atmospheric Administration (NOAA), 2006. 2-Minute Gridded Global Relief Data (ETOPO2v2). U.S. Department of Commerce, National Geophysical Data Center (Retrieved from http://www.ngdc.noaa.gov/mgg/fliers/06mgg01.html).
Natland, J.H., Dick, H.J.B., 2001. Formation of the lower ocean crust and the crystallization of gabbroic cumulates at a very slowly spreading ridge. Journal of Volcanology and Geothermal Research 110 (3–4), 191–233. http://dx.doi.org/10.1016/S0377-0273(01)00211-6.
Neal, C.R., Mahoney, J.J., Chazey, W.J., 2002. Mantle Sources and the Highly Variable Role of Continental Lithosphere in Basalt petrogenesis of the Kerguelen Plateau and Broken Ridge LIP: results from ODP Leg 183. Journal of Petrology 43 (7), 1177–1205. http://dx.doi.org/10.1093/petrology/43.7.1177.
Nicolaysen, K., Frey, F.A., Hodges, K.V., Weis, D., Giret, A., 2000. 40Ar/39Ar geochronology of flood basalts from the Kerguelen Archipelago, southern Indian Ocean: implications for Cenozoic eruption rates of the Kerguelen plume. Earth and Planetary Science Letters 174 (3–4), 313–328. http://dx.doi.org/10.1016/S0012-821X(99)00271-X.
O'Neill, C., Müller, D., Steinberger, B., 2005. On the uncertainties in hot spot reconstructions and the significance of moving hot spot reference frames. Geochemistry, Geophysics, Geosystems 6 (4), Q04003. http://dx.doi.org/10.1029/2004GC000784.
Pearce, J.A., 2008. Geochemical fingerprinting of oceanic basalts with applications to ophiolite classification and the search for Archean oceanic crust. Lithos 100 (1), 14–48.
Pearce, J.A., Norry, M.J., 1979. Petrogenetic implications of Ti, Zr, Y, and Nb variations in volcanic rocks. Contributions to Mineralogy and Petrology 69 (1), 33–47. http://dx.doi.org/10.1007/BF00375192.
Peterson, J.J., Fox, P.J., Schreiber, E., 1974. Newfoundland ophiolites and the geology of the oceanic layer. Retrieved from http://www.nature.com/nature/journal/v247/n5438/abs/247194a0.html.
Pockalny, R.A., Fox, P.J., Fornari, D.J., Macdonald, K.C., Perfit, M.R., 1997. Tectonic reconstruction of the Clipperton and Siqueiros Fracture Zones: Evidence and consequences of plate motion change for the last 3 Myr. Journal of Geophysical Research: Solid Earth (1978–2012) 102 (B2), 3167–3181.
Powell, C.M., Roots, S.R., Veevers, J.J., 1988. Pre-breakup continental extension in East Gondwanaland and the early opening of the eastern Indian Ocean. Tectonophysics 155 (1-4), 261–283.
Ramana, M.V., Ramprasad, T., Desa, M., 2001. Seafloor spreading magnetic anomalies in the Enderby Basin, East Antarctica. Earth and Planetary Science Letters 191 (3), 241–255.
Ribe, N.M., 1997. The dynamics of plume–ridge interaction 2. Off-ridge plumes. Oceanographic Literature Review 4 (44), 334.
Robinson, P.T., Von Herzen, R., Adamson, A., 1988. Leg 118 Preliminary Report, Fracture Zone Drilling on the Southwest Indian Ridge (Preliminary No. Leg 118). Ocean Drilling Program (Retrieved from http://www-odp.tamu.edu/publications/prelim/118PREL.PDF).
Sandwell, D.T., Smith, W.H.F., 2009. Global marine gravity from retracked Geosat and ERS-1 altimetry: Ridge segmentation versus spreading rate. 114, B01411. http://dx.doi.org/10.1029/2008JB006008.
Sempéré, J.C., Cochran, J.R., 1997. The Southeast Indian Ridge between 88 E and 118 E: Variations in crustal accretion at constant spreading rate. Journal of Geophysical Research: Solid Earth 102 (B7), 15489–15505.
Shen, Y., Forsyth, D.W., 1995. Geochemical constraints on initial and final depths of melting beneath mid-ocean ridges. Journal of Geophysical Research—Solid Earth 100 (B2), 2211–2237. http://dx.doi.org/10.1029/94JB02768.
Sleep, N.H., 1996. Lateral flow of hot plume material ponded at sublithospheric depths. Journal of Geophysical Research—Solid Earth 101 (B12), 28065–28083. http://dx.doi.org/10.1029/96JB02463.
Sleep, N.H., 2002. Ridge-crossing mantle plumes and gaps in tracks. Geochemistry, Geophysics, Geosystems 3 (12), 8505. http://dx.doi.org/10.1029/2001GC000290.
Sleep, N.H., 2008. Channeling at the base of the lithosphere during the lateral flow of plume material beneath flow line hot spots. Geochemistry, Geophysics, Geosystems 9 (8), Q08005. http://dx.doi.org/10.1029/2008GC002090.
Small, 1989. An Abrupt Change in Ridge axis Gravity with Spreading Rate. Journal of Geophysical Research-Solid Earth and Planets 94, 17383–17392. http://dx.doi.org/10.1029/JB094iB12p17383.
Small, C., 1995. Observations of ridge-hotspot interactions in the Southern Ocean. Journal of Geophysical Research: Solid Earth 100 (B9), 17931–17946.
Smith, W.H.F., 1998. Seafloor Tectonic Fabric from Satellite Altimetry. Annual Review of Earth and Planetary Sciences 26 (1), 697–747. http://dx.doi.org/10.1146/annurev.earth.26.1.697.
Storey, M., Kent, R.W., Saunders, A.D., Salters, V.J., Hergt, J., Whitechurch, H., et al., 1992. Lower Cretaceous volcanic rocks on continental margins and their relationship to the Kerguelen Plateau. Proceeding of the Ocean Drilling Program, Scientific Results 120, 33–53 (Retrieved from http://www-odp.tamu.edu/publications/120_sr/volume/chapters/sr120_02.pdf).
Sun, S.-S., McDonough, W.F., 1989. Chemical and isotopic systematics of oceanic basalts: implications for mantle composition and processes. Geological Society, London, Special Publications 42 (1), 313–345. http://dx.doi.org/10.1144/GSL.SP.1989.042.01.19.
Sun, S.-S., Nesbitt, R.W., Sharaskin, A.Y., 1979. Geochemical characteristics of mid-ocean ridge basalts. Earth and Planetary Science Letters 44 (1), 119–138. http://dx.doi.org/10.1016/0012-821X(79)90013-X.
Tucholke, B.E., Behn, M.D., Buck, W.R., Lin, J., 2008. Role of melt supply in oceanic detachment faulting and formation of megamullions. Geology 36 (6), 455–458.
Veevers, J.J., Powell, C.M., Roots, S.R., 1991. Review of seafloor spreading around Australia. I. synthesis of the patterns of spreading. Australian Journal of Earth Sciences 38 (4), 373–389. http://dx.doi.org/10.1080/08120099108727979.
Verma, S.P., 1992. Seawater alteration effects on REE, K, Rb, Cs, Sr, U, Th, Pb and Sr-Nd-Pb isotope systematics of Mid-Ocean Ridge Basalt. Geochemical Journal 26 (3), 159–177.
Whittaker, J.M., Müller, R.D., Roest, W.R., Wessel, P., Smith, W.H.F., 2008. How supercontinents and superoceans affect seafloor roughness. Nature 456 (7224), 938–941. http://dx.doi.org/10.1038/nature07573.
Whittaker, J.M., Williams, S.E., Müller, R.D., 2013. Revised tectonic evolution of the Eastern Indian Ocean. Geochemistry, Geophysics, Geosystems 14 (6), 1891–1909. http://dx.doi.org/10.1002/ggge.20120.
Whittaker, J.M., Williams, S.E., Halpin, J.A., Wild, T., Stilwell, J.D., Jourdan, F., Daczko, N.R., 2016. Microcontinent formation driven by plate motion changes (in review).
Williams, S., 2011. Voyage Summary: Southern Surveyor ss2011/v06.
Williams, S.E., Whittaker, J.M., Granot, R., Müller, R.D., 2013. Early India-Australia spreading history revealed by newly detected Mesozoic magnetic anomalies in the Perth Abyssal Plain. Journal of Geophysical Research: Solid Earth 118 (7), 3275–3284. http://dx.doi.org/10.1002/jgrb.50239.
Worthington, T.J., Hekinian, R., Stoffers, P., Kuhn, T., Hauff, F., 2006. Osbourn Trough: Structure, geochemistry and implications of a mid-Cretaceous paleospreading ridge in the South Pacific. Earth and Planetary Science Letters 245 (3–4), 685–701. http://dx.doi.org/10.1016/j.epsl.2006.03.018.
Xu, G., Frey, F.A., Weis, D., Scoates, J.S., Giret, A., 2007. Flood basalts from Mt. Capitole in the central Kerguelen Archipelago: Insights into the growth of the archipelago and source components contributing to plume-related volcanism. Geochemistry, Geophysics, Geosystems 8 (6), Q06007. http://dx.doi.org/10.1029/2007GC001608.
Zhu, D., Mo, X., Pan, G., Zhao, Z., Dong, G., Shi, Y., ... Zhou, C., 2008. Petrogenesis of the earliest Early Cretaceous mafic rocks from the Cona area of the eastern Tethyan Himalaya in south Tibet: Interaction between the incubating Kerguelen plume and the eastern Greater India lithosphere? Lithos 100 (1), 147–173.
Zhu, D.-C., Chung, S.-L., Mo, X.-X., Zhao, Z.-D., Niu, Y., Song, B., Yang, Y.-H., 2009. The 132 Ma Comei-Bunbury large igneous province: Remnants identified in present-day southeastern Tibet and southwestern Australia. Geology 37 (7), 583–586. http://dx.doi.org/10.1130/G30001A.1.